REGULAR ARTICLE

Osteopontin mediates the formation of corpora amylacea-like structures from degenerating neurons in the CA1 region of the rat hippocampus after ischemia

Tae-Ryong Riew[1] · Xuyan Jin[1,2] · Ji-Won Hwang[1] · Soojin Kim[1] · Hong Lim Kim[3] · Mun-Yong Lee[1,2]

Abstract

We previously demonstrated that osteopontin (OPN) is closely associated with calcium precipitation in response to ischemic brain insults. The present study was designed to elucidate the possible association between deposition of OPN and progressive neurodegeneration in the ischemic hippocampus. To address this, we analyzed the OPN deposits in the rat hippocampus after global cerebral ischemia in the chronic phase (4 to 12 weeks) after reperfusion using immunoelectron microscopy and correlative light and electron microscopy. We identified three different types of OPN deposits based on their morphological characteristics, numbered according to the order in which they evolved. Dark degenerative cells that retained cellular morphology were frequently observed in the pyramidal cell layer, and type I OPN deposits were degenerative mitochondria that accumulated among these cells. Type II deposits evolved into more complex amorphous structures with prominent OPN deposits within their periphery and within degenerative mitochondria-like structures. Finally, type III had large concentric laminated structures with irregularly shaped bodies in the center of the deposits. In all types, OPN expression was closely correlated with calcification, as confirmed by calcium fixation and Alizarin Red staining. Notably, type II and III deposits were highly reminiscent of corpora amylacea, glycoprotein-rich aggregates found in aged brains, or neurodegenerative disease, which was further confirmed by ubiquitin expression and periodic acid-Schiff staining. Overall, our data provide a novel link between ongoing neurodegeneration and the formation of corpora amylacea-like structures and calcium deposits in the ischemic hippocampus, suggesting that OPN may play an important role in such processes.

Keywords Osteopontin · Global ischemia · Calcification · Corpora amylacea · Correlative light electron microscopy

Introduction

Osteopontin (OPN) is a phosphorylated acidic glycoprotein linked to various central nervous system (CNS) pathologies, such as the recruitment of multiple inflammatory cell types, modulation of inflammatory responses, matrix remodeling,

and tissue repair (An et al. 2021; Choi et al. 2007; Ellison et al. 1998, 1999; Gliem et al. 2015; Jin et al. 2016; Lee et al. 1999; Meller et al. 2005; Riew et al. 2019; Schroeter et al. 2006; Wang et al. 1998; Yan et al. 2009). OPN also acts as a regulator of ectopic calcification and pathologic mineralization of the brain (Maetzler et al. 2010; Park et al. 2012; Riew et al. 2017; Shin et al. 2011, 2012). After experimentally inducing acute striatal injury using the mitochondrial toxin 3-nitropropionic-acid (3-NP), we have previously demonstrated that OPN-positive staining is visible as small granular puncta, which correspond to calcified mitochondria in degenerated neurites initially and then degenerating calcified neurites by ultrastructural investigation; this indicates that OPN mediates the progression of microcalcification in response to brain insults (Riew et al. 2017).

Brain parenchymal calcification is a well-recognized feature of various neuropathological disorders, including brain ischemia and calcium precipitation in the ischemic

✉ Mun-Yong Lee
munylee@catholic.ac.kr

1 Department of Anatomy, Catholic Neuroscience Institute, College of Medicine, The Catholic University of Korea, 222 Banpo-daero, Seocho-gu, Seoul 06591, Republic of Korea

2 Department of Biomedicine and Health Sciences, College of Medicine, The Catholic University of Korea, Seoul 06591, Republic of Korea

3 Integrative Research Support Center, Laboratory of Electron Microscope, College of Medicine, The Catholic University of Korea, Seoul 06591, Republic of Korea

hippocampus, and it has been ascribed to neuronal death (Bonnekoh et al. 1992; Bueters et al. 2008; Ramonet et al. 2002, 2006). Interestingly, our previous study demonstrated that granular OPN deposits appear first in the stratum radiatum of the CA1 region by 4 weeks after ischemia, followed by protracted and progressive OPN accumulation occurring in the pyramidal cell layer of the CA1 hippocampus over the chronic interval of 8–12 weeks (Park et al. 2012). In this study, ultrastructural studies revealed that these OPN deposits are closely correlated with ectopic calcification processes. Since transient forebrain ischemia causes selective neuronal death in the CA1 hippocampus that commences within 2 to 3 days after ischemia and reaches maximal effects within 1–2 weeks (Kirino and Sano 1984; Pulsinelli et al. 1982; Smith et al. 1984), we questioned whether long-lasting OPN expression in the ischemic hippocampus is related to ongoing neurodegenerative processes rather than early neuronal death at the time of injury. In support of this, progressive neuronal degeneration has been demonstrated in response to brief periods of ischemia or trauma (Bendel et al. 2005; Bueters et al. 2008; Kiryk et al. 2011; Ordy et al. 1993; Radenovic et al. 2020). However, the role of OPN in late-onset neurodegeneration in the ischemic hippocampus remains to be fully elucidated.

Therefore, we defined the exact characteristics and developmental trajectory of OPN-labeled structures and the role of OPN in neurodegenerative processes in the CA1 region of the hippocampus during the late phase (4 to 12 weeks) of brain ischemia. We used several different ultrastructural analyses, including conventional transmission electron microscopy (TEM), electron microscopy using the osmium/potassium dichromate method, pre-embedding immunoperoxidase method, and correlative light and electron microscopy (CLEM). Our results showed that OPN-labeled deposits were compact laminated structures with uniform filamentous materials similar to the corpora amylacea, which are glycoproteinaceous inclusions commonly found during the course of normal aging and in some neurodegenerative diseases, and can act as containers to remove waste products from the brain (Augé et al. 2019; Cavanagh 1999; Navarro et al. 2018; Riba et al. 2019, 2021; Schipper and Cissé 1995; Song et al. 2014). Our results show that OPN is involved in the process of transforming degenerated neuronal debris into corpora amylacea-like structures in the chronic phase after transient ischemia.

Materials and methods

Animal preparation

All experimental protocols and animal care provisions were in accordance with the Laboratory Animals Welfare Act, the Guide for the Care and Use of Laboratory Animals, and the Guidelines and Policies for Rodent Survival Surgery provided by the Institutional Animal Care and Use Committee (IACUC) at the College of Medicine of The Catholic University of Korea (Approval number: CUMS-2020–0041-03). IACUC and the Department of Laboratory Animals (DOLA) at the Catholic University of Korea, Songeui Campus, accredited the Korea Excellence Animal Laboratory Facility of the Korea Food and Drug Administration in 2017 and acquired the full Association for Assessment and Accreditation of Laboratory Animal Care (AAALAC) International accreditation in 2018. All efforts were made to minimize animal suffering and reduce the number of animals used.

Adult male Sprague–Dawley rats (250–300 g, OrientBio, Seongnam, Republic of Korea) were used in this study. The animals were housed in groups of three per cage in a controlled environment at a constant temperature (22 ± 5 °C) and humidity ($50 \pm 10\%$) with food (gamma ray-sterilized diet) and water (autoclaved tap water) available ad libitum. Transient forebrain ischemia was induced by the four-vessel occlusion and reperfusion method described by Pulsinelli and Brierley (1979), with minor modifications (Lee et al. 2002). Briefly, the vertebral arteries were electrocauterized and cut to stop the circulation in these vessels. After 24 h, both common carotid arteries were occluded for 10 min using miniature aneurysmal clips. Body temperatures (measured rectally) were maintained at 37.5 ± 0.3 °C with a heating lamp during and after ischemia. Sham-operated rats with cauterized vertebral arteries and ligatures placed around the carotid arteries were used as controls. The following inclusion criteria were applied: (1) only those animals with an absent righting reflex after vascular occlusion were classified as demonstrating ischemia, and (2) the reduction or absence of neurons in the CA1 region was verified using hematoxylin–eosin-stained sections. None of the sham-operated animals experienced convulsions or died ($n = 18$ rats). After the surgery, animals were monitored twice daily to determine their health and activity levels, including behavioral changes (activity and food intake), body weight, and body temperature. Of the total 48 rats, 44 survived in the ischemic group, and most deaths occurred during or shortly after the ischemic insult, and the leading cause of death appeared to be related to cardiac arrest. However, none of the rats were eliminated from the analysis in the days following the ischemic insult due to sickness or death, and we did not observe any prominent changes in the behavior or body weight of the rats during the experiments.

Animals were sacrificed at 2, 4, 8, or 12 weeks after reperfusion ($n = 5$ rats/time point for the ischemic group; $n = 3$/time point for the sham-operation group). The animals were transcardially perfused with 4% paraformaldehyde in 0.1 M phosphate buffer (PB, pH 7.4) after anesthesia using zolazepam (20 mg/kg i.p.) and xylazine

(7.5 mg/kg i.p.). The brain tissues were equilibrated with 30% sucrose in 0.1 M PB, frozen, and stored at –70 °C for light microscopic study.

Histology and immunofluorescence analysis

For double or triple fluorescence immunohistochemistry, free-floating Sects. (25-µm thick) were blocked in blocking buffer (a mixture of 0.2% gelatine, 1% bovine serum albumin, and 0.05% saponin or a mixture of 10% normal serum, 1% bovine serum albumin, and 0.1% triton) and then incubated at 4 °C overnight with a mix of goat anti-OPN (1:1,000; R&D systems, Minneapolis, MN, USA, AF808), mouse anti-OPN (1:300, American Research Products, Waltham, MA, USA, 01–20,002), rabbit anti-reduced nicotinamide adenine dinucleotide (NADH) dehydrogenase (ubiquinone) flavoprotein 2 (NDUFV2; 1:100; Proteintech, Rosemont, IL, USA, 15,301–1-AP), mouse anti-neuronal nuclear antigen (NeuN; 1:500; Millipore, Temecula, CA, USA, MAB353), rabbit anti-parvalbumin (PV; 1:1,000; Swant, Switzerland, PV 25), and mouse anti-ubiquitin (Ub; 1:100; Santa Cruz Biotechnology, Dallas, TX, USA, sc-8017). To simultaneously detect apoptotic cells, OPN, and NeuN, we performed terminal deoxynucleotidyl transferase dUTP nick end labeling (TUNEL) staining according to the manufacturer's protocol (Roche Diagnostics Corporation, Indianapolis, IN, USA). Antibody or TUNEL staining was visualized using Cy3/Cy5-conjugated donkey anti-goat antibody (1:2,000; Jackson ImmunoResearch, West Grove, PA, USA), Cy3-conjugated streptavidin (1:2,000; Jackson ImmunoResearch), and Alexa 488 donkey anti-rabbit/mouse antibody (1:300; Thermo Fisher, Waltham, MA, USA). Negative staining controls for immunofluorescence involved omission of primary or secondary antibodies. Counterstaining of cell nuclei was carried out using DAPI (4,6-diamidino-2-phenylindole, 1:2000; Roche) for 10 min. Slides were viewed with a confocal microscope (LSM 800 with Airyscan; Carl Zeiss Co. Ltd., Oberkochen, Germany) equipped with four lasers (Diode 405, Argon 488, HeNe 543, HeNe 633). OPN signals were 3D-rendered using IMARIS (Bitplane, Belfast, UK). Images were converted to TIFF format, and contrast levels were adjusted using Adobe Photoshop v.13.0.

To investigate the relationship between calcification and CA deposition, Alizarin Red S, hematoxylin and eosin (H&E), and periodic acid-Schiff (PAS) staining was performed on consecutive hippocampal tissue Sects. (25-µm thick) as described previously (Augé et al. 2018b; Riew et al. 2016). Slides were scanned using a slide scanner (SCN400, Leica Microsystems Ltd., Mannheim, Germany).

Quantitative analysis and statistics

For quantitative analysis, confocal images were obtained with a $40 \times$ (mean intensity of OPN) or $63 \times$ (number of each type of deposit) objective lens under constant viewing settings. To compare mean OPN expression in the hippocampal CA1 region, mean fluorescence intensity from randomly selected areas ($n=6$–8 per animal) with the same size (4,420 μm^2 in x–y and 7.2-µm maximal intensity z-projection) was measured using Zen 2.3 blue (Carl Zeiss Co. Ltd.). To count each type of OPN deposit, we used 67.6×67.6 µm images of 5 µm Z-stacks with 0.3 µm optical sections ($n=3$–5 per animal), counting each type according to the definition described later.

Statistical significance was determined by one-way analysis of variance (ANOVA) followed by Tukey's multiple comparison test. Differences were considered significant at p values less than 0.05. Each p value and the number of animals are presented in the graphs and figure legends. All statistical calculations were performed using Prism 7 (GraphPad Software Inc., San Diego, CA, USA).

Electron microscopic analysis

For the CLEM study, vibratome Sects. (100 µm thick) containing the CA1 region of the hippocampus from control ($n=3$) and ischemic rats at 2, 4, 8, and 12 weeks after reperfusion ($n=3$ rats/time point) were cryoprotected with 2.3 M sucrose in 0.1 M phosphate buffer and frozen in liquid nitrogen. Semi-thin cryosections (2 µm thick) were cut at -100 °C with a glass knife in a Leica EM UC7 ultramicrotome equipped with an FC7 cryochamber (Leica, Wetzlar, Germany). The sections were labeled using mouse anti-OPN (American Research Products, 1:300) or goat anti-OPN (R&D Systems, 1:1,000). Antibody staining was visualized using Cy3-conjugated donkey anti-goat antibody (Jackson ImmunoResearch, 1:2,000) or Alexa594-FluoroNanogold goat anti-mouse antibody (Nanoprobes Inc., Yaphank, NY, USA, 1:100). The sections were labeled with DAPI for 10 min. Coverslipped sections were examined with a confocal microscope and photographed at various magnifications with a differential interference contrast setting to identify specific areas for later examination by electron microscopy. After the coverslips had been floated off the sections, the tissues were prepared for TEM as described previously (Kim et al. 2021; Riew et al. 2019). After post-fixation, dehydration, and embedding in epon 812 (Polysciences, Warrington, PA, USA), areas of interest were excised and glued onto resin blocks. After being cut into ultrathin sections of 70–90 nm thickness, they were observed using an electron microscope (JEM 1010; JEOL, Tokyo, Japan) with slight uranyl acetate staining.

For pre-embedding immunoelectron microscopy, floating vibratome Sects. (50 μm thick) from control ($n = 3$) and ischemic rats at 2, 4, 8, and 12 weeks after reperfusion ($n = 3$ rats/time point) were immunostained with mouse anti-OPN (1:300, American Research Products) or goat anti-OPN (1:1,000, R&D Systems). Immunoreactions were visualized using peroxidase-labeled donkey anti-mouse or donkey anti-goat IgG (Jackson ImmunoResearch, 1:150) and 0.05% 3,3-diaminobenzidine tetrahydrochloride (DAB) as a chromogen. The tissues were prepared for electron microscopy as described above.

For conventional TEM, vibratome Sects. (50 μm thick) from control ($n = 3$) and ischemic rats at 2, 4, 8, and 12 weeks after reperfusion ($n = 3$ rats/time point) were postfixed with 2.5% glutaraldehyde and 1% osmium tetroxide (OsO_4). For calcium fixation, vibratome Sects. (50 μm thick) from control ($n = 3$) and ischemic rats at 2, 4, 8, and 12 weeks after reperfusion ($n = 3$ rats/time point) were postfixed in 1% osmium tetroxide (OsO_4) and 2.5% potassium dichromate ($K_2Cr_2O_7$; Hayashi Pure Chemical Industries Ltd., Osaka, Japan) for 1 h at 4 °C (Probst 1986). The tissues were prepared for TEM as described above. Semi-thin (500 nm thick) sections from embedded tissues were further stained with toluidine blue to visualize corpora amylacea-like structures in the pyramidal cell layer of the hippocampus (Morikawa et al. 2018; Trump et al. 1961).

Results

Characterization and time-dependent changes of OPN-positive deposits in the pyramidal cell layer of the ischemic CA1 hippocampus

We first characterized OPN-immunoreactive profiles within the vulnerable CA1 hippocampus during the 12 weeks after transient forebrain ischemia. No specific staining for OPN was detected in the CA1 hippocampus of sham-operated rats (Fig. 1a), but at 2 weeks after ischemia, tiny granular deposits showing OPN immunoreactivity were diffusely distributed in the dendritic subfields including the stratum oriens and radiatum, but not in the pyramidal cell layer of the CA1 region (Fig. 1b), consistent with our previous observations (Choi et al. 2007; Park et al. 2012). Four weeks after ischemia, non-diffuse OPN profiles of various shapes and sizes were detected in the pyramidal cell layer of the CA1 hippocampus, which became more pronounced over time (Fig. 1c–e). We assessed the relative intensity of OPN expression within the pyramidal cell layer of the CA1 hippocampus during the injury period. The intensity did not change until 2 weeks after the onset of ischemia but significantly increased by 4 weeks, and the enhanced expression

was maintained until at least the latest time point examined (12 weeks; Fig. 1f).

As shown in higher magnification images of the CA1 pyramidal cell layer, OPN immunostaining was negligible by 2 weeks after the onset of ischemia (Fig. 1g) but was visible as small puncta to larger deposits of various sizes and shapes over the chronic interval of 4–12 weeks (Fig. 1h–j). Using light microscopy, OPN staining could be divided into three distinct types according to morphological characteristics. Type I OPN deposits showed granular puncta localized to the shape of cells that had nuclei weakly labeled with DAPI (Fig. 1k), which was corroborated by the 3D reconstructed images (Fig. 1l). Type II OPN deposits were characterized by structures that were larger and highly variable in size and shape; they were not limited to cell boundaries but instead appeared as clusters of cells (Fig. 1m). Type III OPN deposits were smooth-outlined, concentrically laminated structures in which intense OPN expression was detected at the periphery and in the core region (Fig. 1n).

Ultrastructural characterization of type I OPN deposits in the pyramidal cell layer of the ischemic CA1 hippocampus

As shown in Fig. 1, type I OPN deposits, visible as granular puncta, were localized within cellular profiles whose nuclei showed weak or barely visible DAPI signal, reminiscent of degenerated cells; they were not observed around strongly DAPI-labeled nuclei (Fig. 2a, b). Thus, we determined whether OPN expression was closely correlated with cell death. TUNEL assay coupled with OPN and the nuclear stain DAPI showed that the weakly labeled nuclei were positive for the cell death marker TUNEL and were surrounded by type I OPN deposits, indicating that type I OPN deposits were localized over the cytoplasm of dying or dead cells (Fig. 2c–e).

We then defined the precise subcellular localization of type I OPN deposits using the CLEM approach. Semi-thin sections labeled for OPN were first observed using confocal microscopy and were subsequently subjected to electron microscopy. Overlay of the confocal microscopy and TEM data showed that type I OPN deposits were located within electron-dense dark cells with homogeneously condensed nuclei, which were degenerated to the extent of precluding cell type identification (Fig. 2f–h). In these cells, OPN staining was likely to be of cell organelles with an electron-dense outline, some of which were presumed to be mitochondria due to their recognizable cristae (Fig. 2i–m). Interestingly, OPN staining was not observed in the adjacent mitochondria-like structures without a distinct electron-dense outline (Fig. 2j).

We further clarified the cellular identity of type I OPN deposits using pre-embedding immunoelectron microscopy. OPN expression was observed in shrunken dark cells
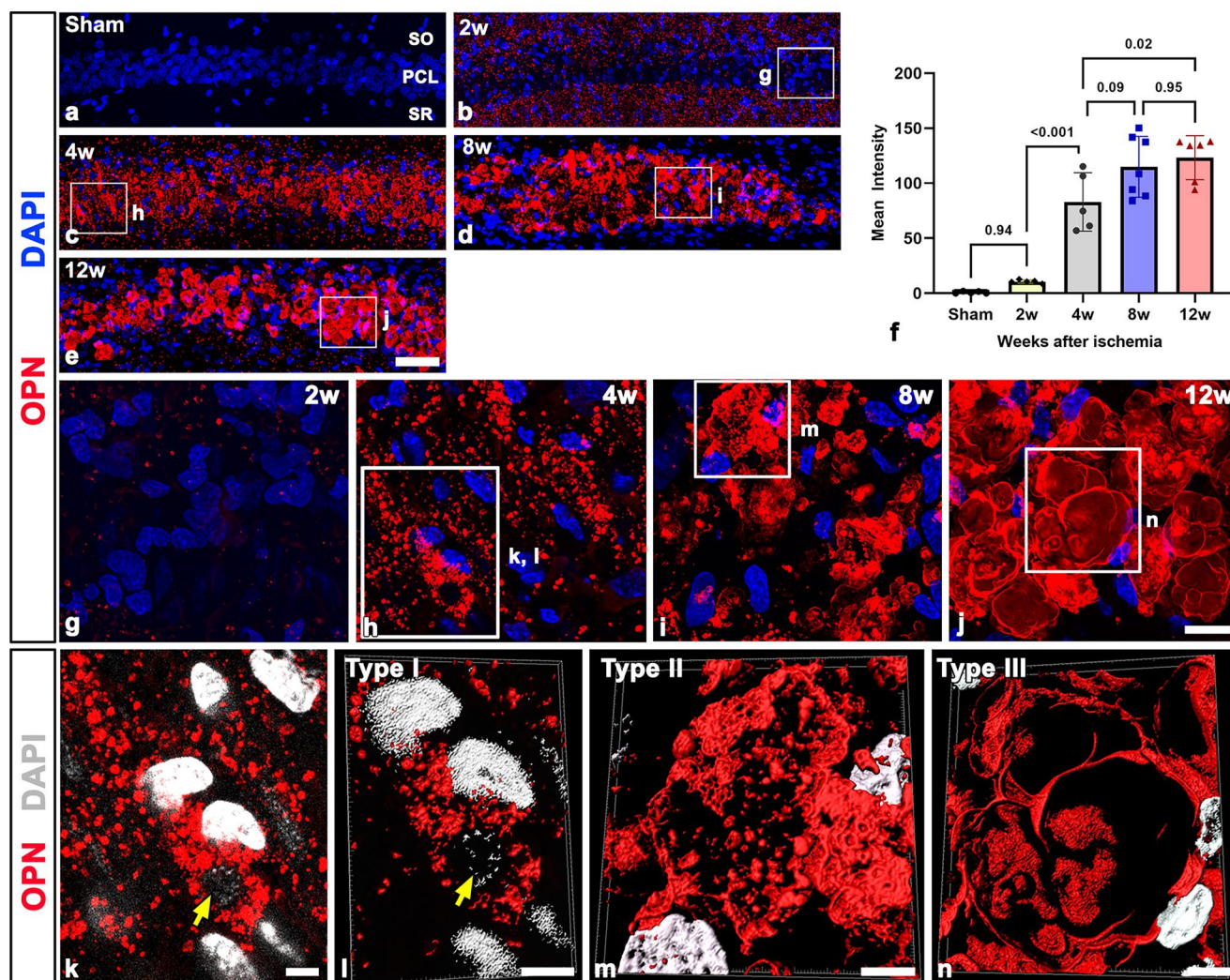
Fig. 1 Representative images showing the temporal profile of OPN-positive deposits in the hippocampal CA1 region after transient forebrain ischemia. (**a**) In control sections, no specific OPN expression was detected in the CA1 hippocampus including the stratum oriens (SO), stratum radiatum (SR), and the pyramidal cell layer (PCL). (**b**) At 2 weeks after ischemia, tiny granular OPN deposits were diffusely distributed over the strata oriens and radiatum, but not in the pyramidal cell layer. (**c–e**) Over the chronic interval of 4 (**c**), 8 (**d**), and 12 weeks (**e**) after ischemia, non-diffuse OPN deposits of variable shape and size were observed in the pyramidal cell layer. (**f**) Quantitative analysis of the intensity of OPN expression in the CA1 pyramidal cell layer in sham-operated control and ischemic rats. Note that the mean intensity of OPN expression significantly increased at 4 weeks, and this enhanced expression was maintained for up to 12 weeks ($n = 6$–8 areas from 5 to 7 rats per group, one-way ANOVA with Tukey's multiple comparison test). The data are expressed as mean ± SEM and the numbers on each bar indicate the p values. (**g–j**) Higher magnification views of the boxed areas in **b–e**, respectively, showing that OPN immunostaining in the CA1 pyramidal cell layer was negligible at 2 weeks (**g**), but was visible as small puncta to larger deposits of various shapes and sizes over the chronic interval of 4–12 weeks (**h–j**). The boxed areas in **h–j** were enlarged in **k–n** and were shown as 3D-rendered images in **l–n**, respectively. Note that three types of OPN deposit were distinguished according to their morphological characteristics. (**k, l**) Type I OPN deposits showed granular puncta localized to the shape of cells, whose nuclei were weakly labeled by DAPI (yellow arrows). (**m, n**) Notably, type II OPN deposits were structures highly variable in size and shape, which appeared to be clusters of cells rather than being located within cell boundaries (**m**), while type III OPN deposits were smooth-outlined, concentrically laminated structures, in which intense OPN expression was detected at the periphery and in the core region. DAPI was used for nuclear counterstain. Scale bars = 50 μm for **a–e**; 10 μm for **g–j**; 4 μm for **k–n**

that had homogeneous nuclei with small spots of scattered condensed chromatin, as well as altered and unidentifiable organelles (Fig. 3a, b). As shown at higher magnifications (Fig. 3b, c), OPN protein, as indicated by highly electron-dense DAB grains, was distributed around the degenerated

mitochondria that still had recognizable internal cristae. These OPN-positive mitochondria appeared smaller and more electron-dense than the adjacent unlabeled mitochondria (Fig. 3c). In advanced degenerated cells with irregularly shaped nuclei and few recognizable organelles, OPN
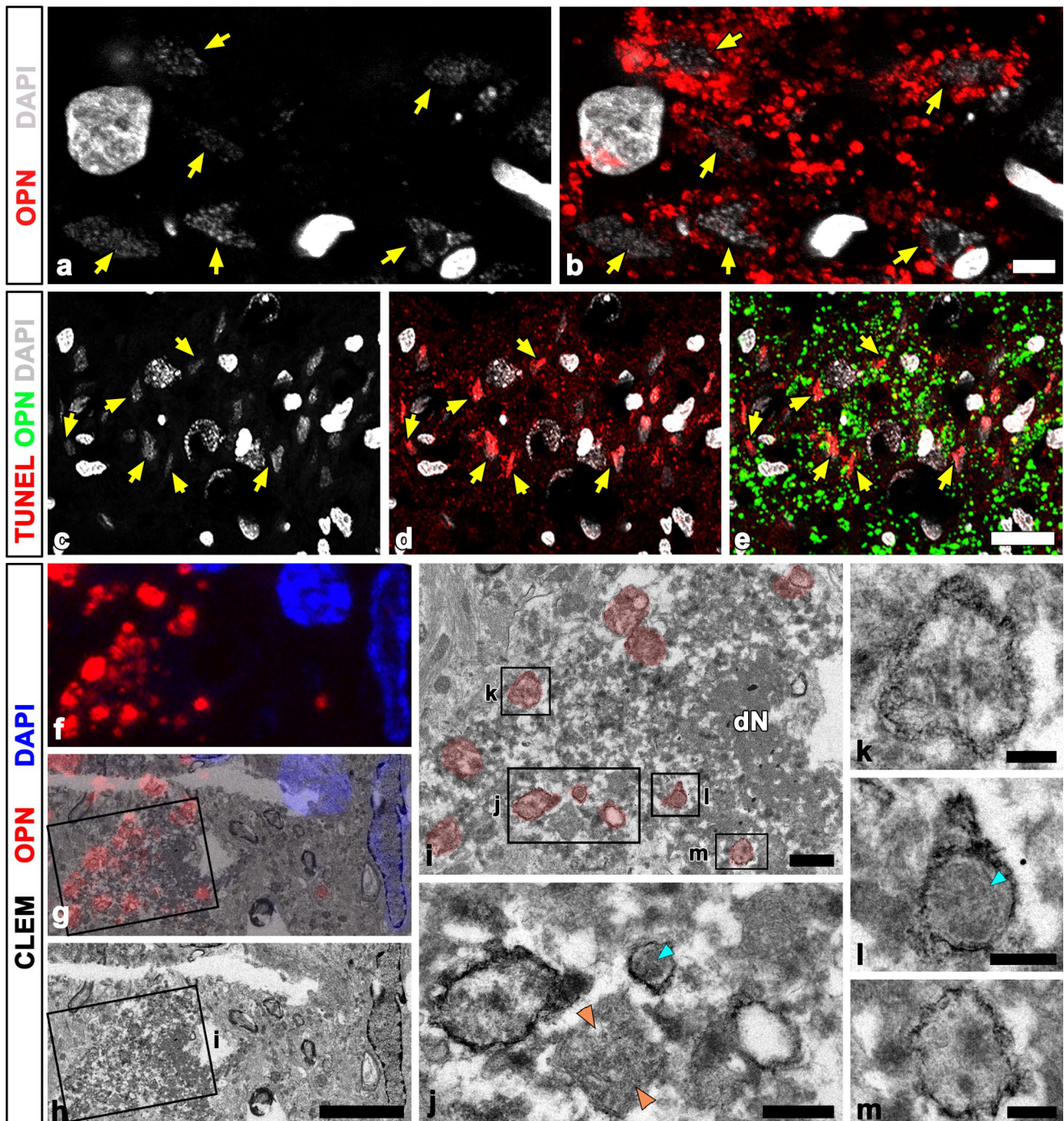
Fig. 2 Ultrastructural identification of type I OPN deposits in the pyramidal cell layer of the ischemic CA1 hippocampus. (**a**, **b**) Type I OPN deposits, visible as granular puncta, were localized around weakly labeled nuclei by DAPI (yellow arrows) within cellular profiles. (**c**–**e**) Double labeling of OPN and TUNEL showing that OPN was localized to the perinuclear region of TUNEL-positive nuclei (yellow arrows) that were weakly labeled by DAPI. (**f**–**h**) Representative correlative light and electron microscopic images. Confocal microscope image of a semi-thin section labeled for OPN (**f**), the overlay image of the confocal microscope data (**g**), and the corresponding electron microscope image (**h**). (**i**) Higher magnification image of the boxed area in **h**, showing an electron-dense dead cell with a homogeneously condensed nucleus (dN). The boxed areas in **i** were enlarged in **j**–**m**, respectively, showing that OPN staining was presumed to be mitochondria with electron-dense outline, some of which retained their cristae structures (blue arrowheads in **j** and **l**). Note that OPN was not associated with mitochondria-like structures without a distinct electron-dense outline (orange arrowheads in **j**). DAPI was used for nuclear counterstain. Scale bars = 5 μm for **a**–**b**; 20 μm for **c**–**e**; 5 μm for **f**–**h**; 1 μm for **i**; 0.5 μm for **j**; 0.25 μm for **k**–**m**

staining was localized to the peripheral outline of unrecognizable structures (Fig. 3d, e), which were similar to degenerated mitochondria in their distribution and shape (Fig. 3c).

We have previously demonstrated that OPN protein is initially localized within the mitochondria of degenerating calcified neurites in the lesioned striatum (Riew et al. 2017). Thus, we examined whether mitochondrial OPN expression was closely related to calcium deposition using the osmium/potassium dichromate method to precipitate and ultrastructurally visualize endogenous calcium (Probst 1986). Electron-dense degenerated cells with homogeneous nuclei frequently contained calcifying structures, in which densely packed needle-shaped calcium crystals were present in the interior and more intense calcium signals were localized to the peripheral outline (Fig. 3f, g). In advanced degenerated cells, these calcifying structures appeared to increase in size and number and became more electron-dense (Fig. 3h, i). The distribution pattern, shape, and size of these calcifying profiles were all remarkably similar to those of OPN-labeled mitochondria observed by immunoelectron microscopy (compare Fig. 3c, e with Fig. 3g, i). Thus, our data indicate that the type I OPN deposits were indeed calcifying mitochondria in dying or dead cells, and that in these mitochondria OPN protein was mainly localized on their periphery.

Phenotypic identification of type I OPN deposit-laden cells in the pyramidal cell layer of the ischemic CA1 hippocampus

Hippocampal interneurons, particularly PV interneurons, can survive at early time points after an ischemic insult, although they undergo degenerative changes following complete loss of CA1 pyramidal neurons (Himeda et al. 2005). To clarify the phenotypes of type I OPN deposit-laden cells, we performed triple labeling for OPN, TUNEL, and PV in ischemic rats perfused for 4 weeks. In the CA1 hippocampus of sham-operated rats, PV labeling was intense in the pyramidal cell layer, which was devoid of specific staining for OPN and TUNEL (Fig. 4a–d). Four weeks after ischemia, PV expression was notably decreased and was virtually absent in type I OPN laden cells and TUNEL-positive cells in the pyramidal cell layer of CA1 hippocampus (Fig. 4e–h). To further clarify whether type I OPN deposit-laden cells corresponded to degenerating neurons, we performed triple labeling for OPN, NeuN, and TUNEL. In the CA1 pyramidal cell layer reperfused for 4 weeks, TUNEL-positive cells with cytoplasm filled with type I OPN deposits were devoid of the neuronal marker NeuN (Fig. 4i–l). Since NeuN antigenicity is readily reduced in neurons after brain injury (Unal-Cevik et al. 2004), it is likely that the loss of neuronal nuclear protein in these cells may result from advanced degenerative changes. Thus, we performed triple labeling for OPN, NeuN, and TUNEL in rats reperfused for 2 weeks. Although

several TUNEL-positive cells were already present in the CA1 pyramidal cell layer, and some of them still expressed NeuN, they were devoid of significant OPN immunoreactivity (Fig. 4m–p). We further examined these degenerating neurons 2 weeks after ischemia at the ultrastructural level. Conventional electron microscopy revealed that dark degenerating neurons were scattered throughout the CA1 pyramidal cell layer among normally appearing neurons, astrocytes, and microglial cells (Fig. 4q–s). They had homogeneous nuclei and highly disorganized cell organelles but conserved nuclear and cytoplasmic membrane conformations (Fig. 4q–s). Their ultrastructural characteristics were remarkably similar to those of type I OPN deposit-laden cells, except that they had no recognizable electron-dense structures (compare Fig. 4q–s with Figs. 2i and 3a), probably indicating that the latter corresponded to dying or dead neurons.

Ultrastructural characterization of type II OPN deposits in the pyramidal cell layer of the ischemic CA1 hippocampus

Next, we examined type II OPN deposits using a CLEM approach. As shown in Fig. 1i and m, confocal microscopic images showed that they had structures variable in size and shape, in which OPN was distinctively expressed along the periphery and was also visible as dots scattered in the interior (Fig. 5a). Overlay of the confocal and TEM images demonstrated that type II OPN deposits were large irregularly shaped structures with shapes reminiscent of degenerating cellular debris, which were composed of a thin and compact outer layer and a less dense inner layer (Fig. 5b, c). In particular, the inner layer had multiple hole-like structures, some of which contained electron-dense mitochondria-like profiles (Fig. 5d–f). The precise localization of OPN within dark cellular debris was further analyzed by CLEM using a fluoro-nanogold secondary antibody. As shown in Fig. 5g–k, overlay of the confocal microscopy and TEM data confirmed that OPN protein, as indicated by silver-enhanced immunogold particles, was specifically localized to the surface of the outer compact layer of the debris and within their hole-like structures. These latter structures showed OPN signals on their peripheral outline and mitochondria-like profiles inside.

Pre-embedding electron microscopic images immunostained with OPN showed irregularly shaped structures composed of nuclear chromatin-like materials in the center and outer cytoplasmic parts with high electron density (Fig. 6a). The latter had several electron-transparent holes containing small, electron-dense mitochondria-like structures (Fig. 6a, b). Within these structures, electron-dense DAB grains were evident along their periphery, within the wall, and mitochondria-like structures of the holes (Fig. 6a,
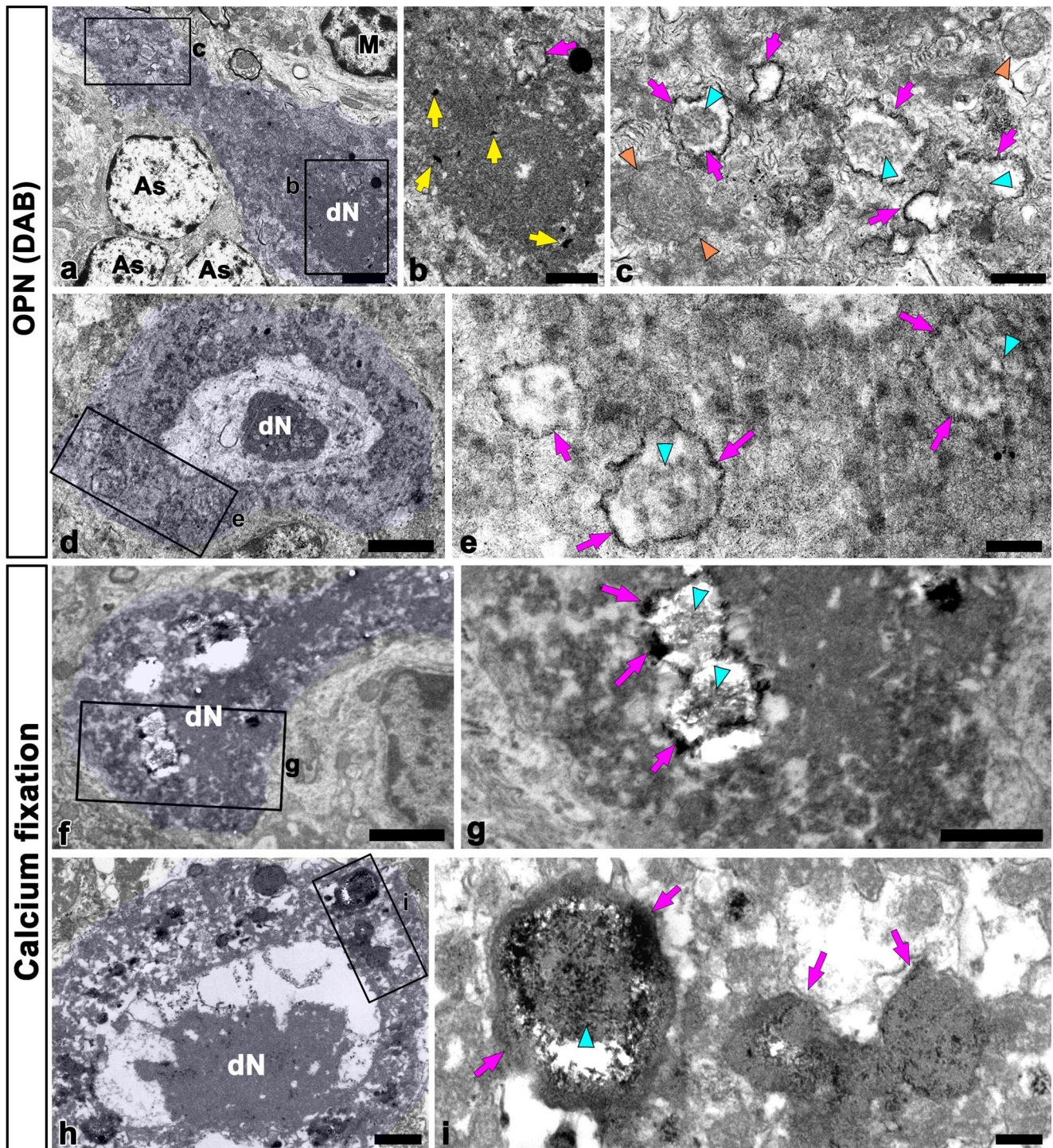
b). Next, we performed a comparative ultrastructural study using the osmium/potassium dichromate method. As shown in Fig. 6c, the calcified bodies shared ultrastructural features similar to those of type II OPN deposits, as shown in Fig. 6a. Higher magnification images showed that needle-like or rod-like calcium crystals were present throughout the entire structure of the calcified bodies, and more intense calcium

crystals were localized on their peripheral outline and within mitochondria-like structures (Fig. 6c, d).

To investigate whether OPN was indeed associated with the mitochondria in degenerating cells, we performed double labeling for OPN and NDUFV2, an enzyme present in the inner mitochondrial membrane (de Coo et al. 1995). In the type I OPN deposits, the distribution of the OPN-positive

◄**Fig. 3** Ultrastructural identification of type I OPN deposits in the pyramidal cell layer of the CA1 hippocampus by comparison of pre-embedding immunoelectron microscopy and the osmium/potassium dichromate method. (**a**) Low magnification view showing a dark cell that had a homogeneous nucleus (dN) and highly disorganized cell organelles, adjacent astrocytes (As), and microglia (M). (**b**, **c**) Higher magnification views of the boxed areas in **a**. OPN immunoreactivity, as indicated by highly electron-dense 3,3′-diaminobenzidine tetrahydrochloride (DAB) grains, was specifically localized to the peripheral outline (magenta arrows in **b** and **c**) of the degenerated mitochondria (blue arrowheads in **c**) that still had recognizable internal cristae. Note that OPN-positive mitochondria appeared small and electron-dense, while the apparently normal mitochondria (orange arrowheads) did not express OPN. Yellow arrows in **b** denote small spots of condensed chromatin scattered in nucleus. (**d**, **e**) Lower (**d**) and higher (**e**) magnification views, showing an advanced degenerated cell that had nuclear chromatin-like materials (dN) and few recognizable organelles. Note that OPN staining was localized to the peripheral outline (magenta arrows in **e**) of mitochondria-like profiles (blue arrowheads in **e**). (**f**–**i**) Representative images acquired using the osmium/potassium dichromate method, showing degenerated cells that had homogeneous nuclei (dN) and contracted dark perikarya with unrecognizable cell organelles. (**g**, **i**) Higher magnification views of the boxed areas in **f** and **h**, respectively. Note that electron-dense precipitates, typical of calcium deposits, were associated with what appeared to be mitochondria, in which calcium signals were found in the interior (blue arrowheads in **g** and **i**) and at the periphery (magenta arrows in **g** and **i**). Scale bars = 2 μm for **a**, **d**, **f**; 1 μm for **b**, **g**, **h**; 0.5 μm for **c**, **e**; 0.2 μm for **i**

puncta overlapped with that of the mitochondrial marker NDUFV2 (Fig. 6e–g). In the type II OPN deposits, OPN dots scattered in the interior were co-labeled with NDUFV2, although OPN expression distributed along their periphery was not associated with NDUFV2 (Fig. 6h–j).

Ultrastructural characterization of type III OPN deposits in the pyramidal cell layer of the ischemic CA1 hippocampus

As shown in Fig. 1j and n, confocal microscopy revealed that type III OPN deposits were seemingly laminated structures, in which OPN was intensely expressed at the periphery and in a punctate pattern on the inside (Fig. 7a). Overlay of the confocal and TEM images demonstrated that type III OPN deposits were acellular smooth-outlined structures, the periphery of which consisted of alternate concentric laminated structures with uniform fibrils, while the center showed fewer compact fibrils and contained electron-dense bodies with various features (Fig. 7b–e).

Pre-embedding immunoelectron microscopy showed that OPN-labeled structures were large irregularly shaped bodies consisting of a homogeneous periphery and central part with electron-dense particles of various shapes (Fig. 7f). In these structures, OPN staining was intense in the periphery and in the central irregularly shaped bodies (Fig. 7f, g). In addition, small round acellular bodies appeared to be attached to their periphery (Fig. 7f). A comparative ultrastructural study

using the osmium/potassium dichromate method showed that large calcifying deposits appeared to be a conglomerate of adjacent calcifying bodies that were fused to each other (Fig. 7h). Needle-like calcium crystals were present throughout the entire structure of the calcified bodies, in which more intense calcium crystals were localized along the periphery and unidentifiable profiles inside (Fig. 7h, i). Interestingly, using conventional TEM we often found what appeared to be calcifying bodies. As shown in Fig. 7j and k, they were composed of compacted and laminated structures, which were more pronounced in the periphery and contained degenerated condensed nuclei in the center, indicating that they shared similar ultrastructural features with OPN-labeled calcified bodies.

Quantitative temporal analysis of the three types of OPN deposits in the pyramidal cell layer of the ischemic CA1 hippocampus

We examined the distribution of three types of OPN deposits in the CA1 hippocampus of reperfused rats at 8 weeks using conventional TEM. Toluidine blue-stained semi-thin sections of the pyramidal cell layer showed numerous structures considered to be OPN deposits of various sizes and shapes (Fig. 8a, b). When adjacent ultrathin sections from the same epon blocks were examined by conventional TEM, all types of OPN deposits were observed in the CA1 pyramidal cell layer of the same animal (Fig. 8c–e). We subsequently quantified the time-dependent changes in each of the three OPN deposits in the CA1 pyramidal cell layer of ischemic rats during the injury period from 4 to 12 weeks based on the classification criteria as described in Table 1. As shown in Fig. 8f–h, the number of type I deposits in the pyramidal cell layer gradually decreased from 4 to 12 weeks after ischemia, while both type II and III deposits showed opposite patterns throughout the injury period. Both type II and III deposits were rarely detected at 4 weeks, while type II was dominant at 8 weeks and type III at 12 weeks. In particular, the number of type III deposits at 12 weeks following ischemia was 17.50 ± 5.08, which was higher than those of type I (1.21 ± 1.10, $p < 0.001$) and type II (10.13 ± 3.05, $p = 0.01$). These results indicated that type II and III deposits showed a tendency to increase in number with time after ischemia, and type III was particularly pronounced.

Relationship between the OPN deposits and corpora amylacea in the pyramidal cell layer of the ischemic CA1 hippocampus

Our data showed that the OPN deposits were similar to corpora amylacea in the ultrastructural morphology in that both were composed of tightly aggregated fibrils with a
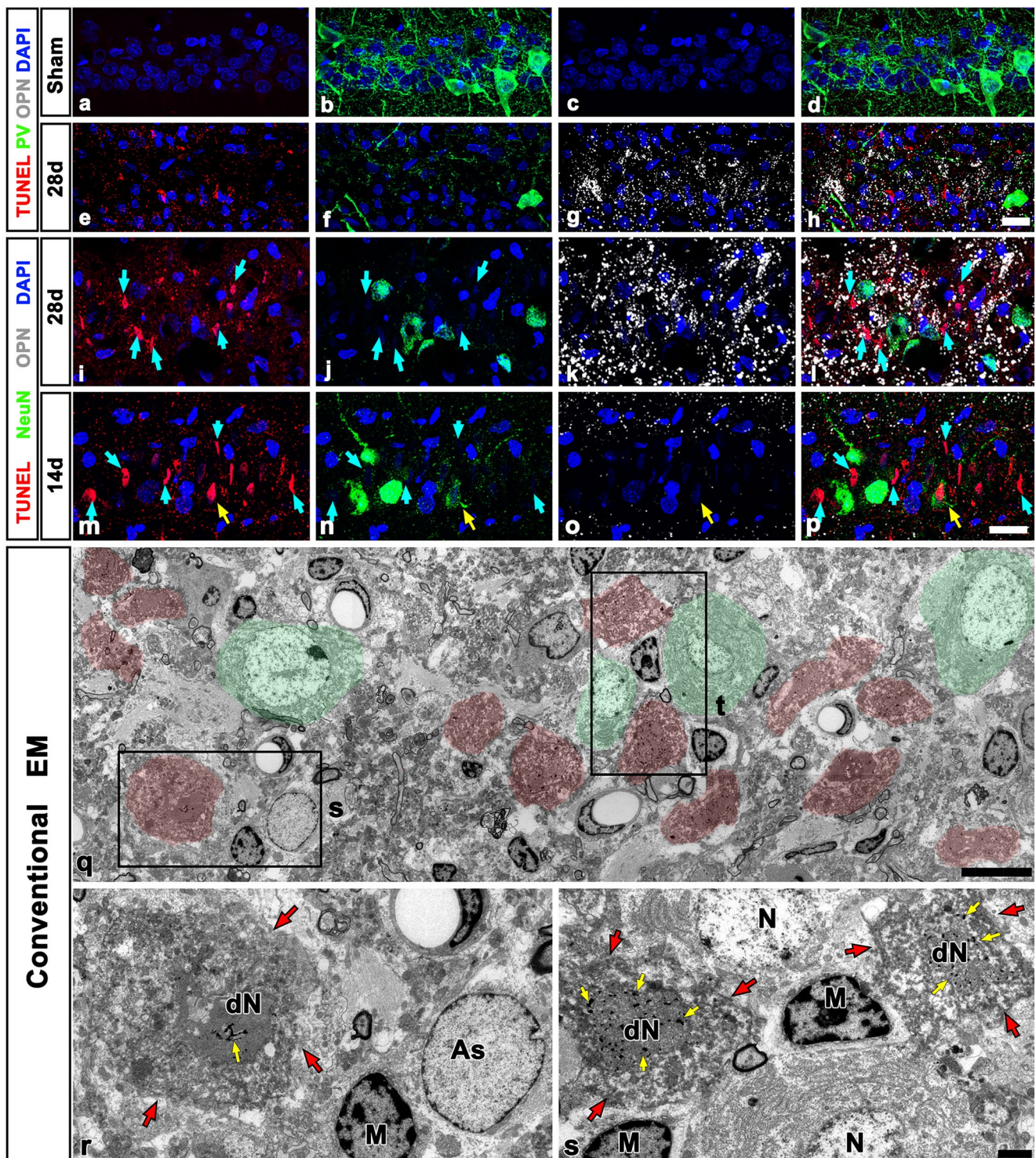
concentrically laminated layer and contained morphologically preserved mitochondria (Augé et al. 2019; Navarro et al. 2018; Riba et al. 2019). To define the relationship between OPN deposits and corpora amylacea in the ischemic hippocampus, we performed H&E and PAS staining to identify

corpora amylacea (Manich et al. 2016) and Alizarin Red staining for calcified OPN deposits (Mori et al. 2000; Nitsch and Scotti 1992) using serial sections from the ischemic hippocampus at 12 weeks post-ischemia. As shown in Fig. 9a–c, ovoid to round calcium deposits of various sizes, which were

◀**Fig. 4** Phenotypic identification of type I OPN deposit-laden cells in the pyramidal cell layer of the ischemic CA1 hippocampus. (**a–d**) Triple labeling of OPN, TUNEL, and parvalbumin (PV) in control tissue sections, showing that neither OPN nor TUNEL was labeled, while PV was intensely labeled in neuronal soma and neurites. (**e–h**) Triple labeling of OPN, TUNEL, and PV in ischemic rats perfused for 4 weeks, showing that PV expression was notably decreased and was virtually absent in type I OPN laden cells and TUNEL-positive cells. (**i–l**) Triple labeling of OPN, TUNEL, and NeuN in the CA1 pyramidal cell layer reperfused for 4 weeks, showing that OPN was localized to the perinuclear region of TUNEL-positive cells (blue arrows) that were not labeled by NeuN. (**m–p**) Triple labeling of OPN, TUNEL, and NeuN in the CA1 pyramidal cell layer reperfused for 2 weeks, showing that TUNEL-positive cells (blue arrows) were devoid of significant OPN immunoreactivity. Note that some TUNEL-positive cells (yellow arrows) still expressed NeuN. (**q–s**) Conventional electron microscopic images of the CA1 pyramidal cell layer reperfused for 2 weeks, showing that degenerating neurons (shaded in red) were scattered among normal-appearing neurons (shaded in green), astrocytes (As), and microglial cells (M). The boxed areas in **q** were enlarged in **r** and **s**, respectively. Note that degenerating neurons had homogeneous nuclei (dN) with small spots of condensed chromatin (yellow arrows) and highly disorganized cell organelles but conserved conformations of nuclear and cytoplasmic membranes. Red arrows mark the boundaries of degenerative cells. DAPI was used for nuclear counterstain. Scale bars = 20 µm for **a–p**; 10 µm for **q**; 2 µm for **r–s**

stained an orange-red color by Alizarin Red, were noted in the CA1 pyramidal cell layer, which corresponded well with that of OPN immunostaining, as reported previously (Park et al. 2012). Routine H&E staining showed the characteristic loss of hippocampal CA1 neurons after transient forebrain ischemia, as described previously (Pulsinelli and Brierley 1979), but also extracellular purple-colored aggregates in the CA1 pyramidal cell layer (Fig. 9d–g). In addition, PAS staining revealed extracellular pink-colored aggregates in the CA1 pyramidal cell layer (Fig. 9g–i). The distribution pattern, shape, and size of calcium deposits detected by Alizarin Red staining in the ischemic hippocampus were remarkably similar to those of both H&E-stained aggregates and PAS-reactive deposits, indicating that OPN-positive deposits in the ischemic hippocampus could correspond to corpora amylacea. Since ubiquitin is detected in corpora amylacea and is considered a marker of corpora amylacea (Augé et al. 2018a; Cissé et al. 1991; Song et al. 2014), we performed double labeling of OPN and ubiquitin to further clarify the relationship between OPN deposits and corpora amylacea. As shown in Fig. 9j–l, ubiquitin was mainly localized in the central part of the OPN-positive deposits.

Discussion

We have previously reported that granular OPN deposits are followed by progressive OPN accumulation in the CA1 hippocampus after global cerebral ischemia, which is closely correlated with spatiotemporal progression of calcification (Park et al. 2012). In the present study, we performed a detailed ultrastructural analysis and defined the exact characteristics and developmental trajectory of OPN-labeled structures occurring in the pyramidal cell layer of the CA1 hippocampus over the chronic interval of 4–12 weeks after ischemia. Thus, our data further support the link between OPN expression and ectopic calcification during ischemic insults and provides a novel insight into the potential role of OPN in the processing of the degenerative neurons into the formation of corpora amylacea-like structures in the ischemic hippocampus.

Notably, we identified three different types of OPN deposits based on their morphological characteristics in the CA1 hippocampus in the chronic phase following transient ischemia (Table 1, Fig. 10). Type I OPN deposits were degenerative, calcified mitochondria that accumulated among dark cellular debris, retaining cellular morphology. Type II deposits were calcified dead cells with amorphous structures, where OPN expression was prominent on their peripheral outline and within degenerative mitochondria-like structures. Type III deposits were large calcifying deposits with concentric laminated structures, intense OPN expression at the periphery, and irregularly shaped bodies in the center of the deposits. Our data revealed that ultrastructural features of the three types of OPN deposits were similar to each other but showed gradual changes from type I to type III, suggesting that the number of each type of OPN deposit indicates the order in which the ultrastructural changes evolve. In particular, the quantitative temporal analysis of the three OPN deposits revealed that the number of type I deposits gradually decreased from 4 to 12 weeks after ischemia, while type II and III deposits, particularly type III, showed a tendency to increase in number with time after ischemia. This might provide, at least in part, the possibility of successive progression of the three types. Additionally, the difference of NDUFV2 staining in type I and II deposits suggests the possibility of transition from type I to type II. However, it is not clear whether the three types of OPN deposits proceed in succession, that is, whether they are directly related to changes as cellular damage progresses; thus, further studies are required to determine the precise mechanisms by which OPN deposits are formed, particularly in relation to neurodegeneration that occur in the ischemic hippocampus.

It is well known that delayed death of hippocampal CA1 pyramidal neurons starts within 2 to 3 days after transient forebrain ischemia and reaches its maximal effect within 1–2 weeks (Kirino and Sano 1984; Pulsinelli et al. 1982; Smith et al. 1984). Although relatively few studies have described cell death persisting to the chronic stages even after 2 weeks following transient ischemic insult, we have
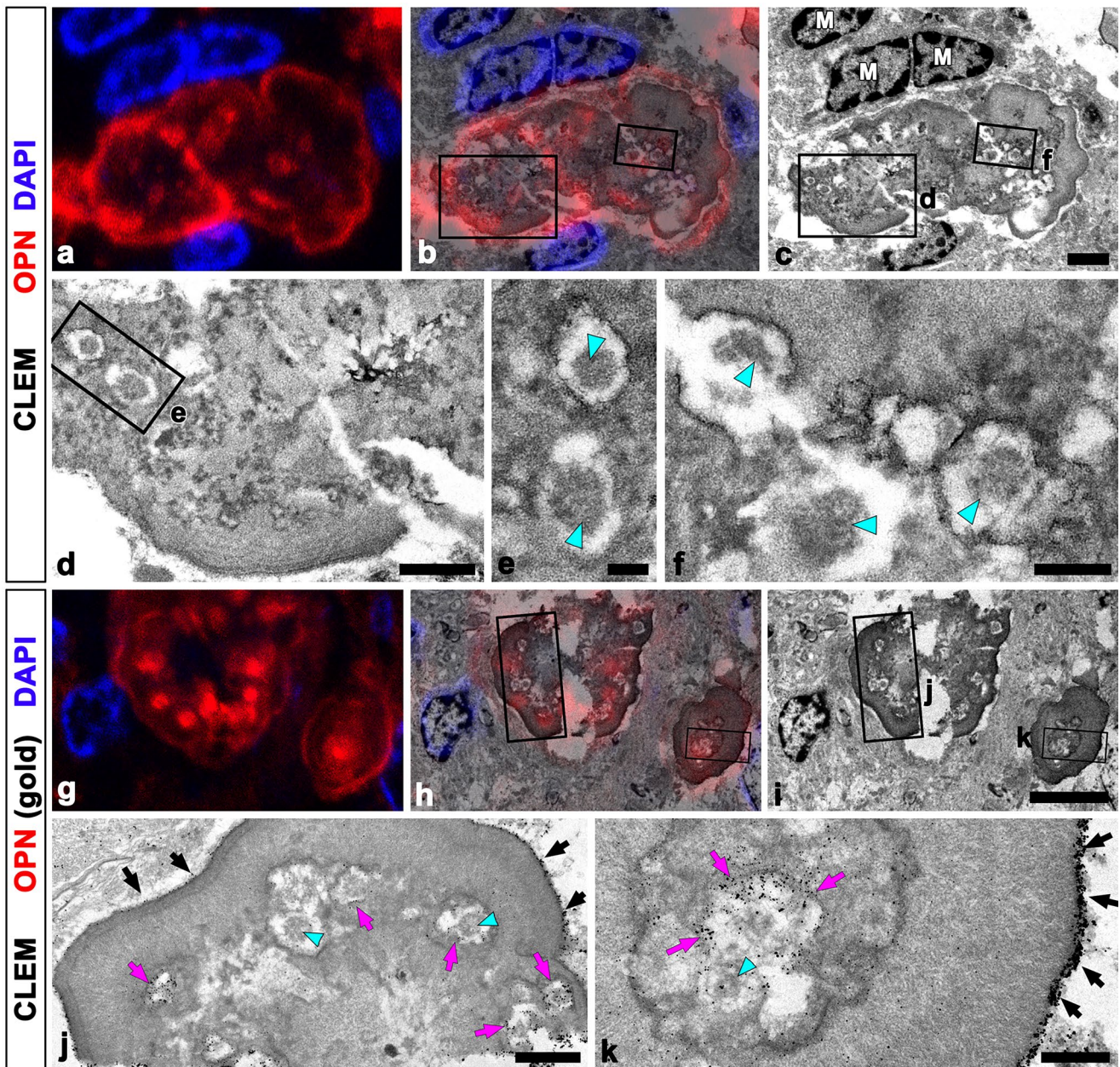
Fig. 5 Ultrastructural identification of type II OPN deposits in the pyramidal cell layer of the CA1 hippocampus using a correlative light and electron microscopy. (**a–c**) Confocal microscope images of a semi-thin section labeled for OPN (**a**), the overlay image of the confocal microscope data (**b**), and the corresponding electron microscope image (**c**). (**d–f**) Higher magnification image of the boxed area in **c** and **d**, respectively. Notably, type II OPN deposits were irregularly shaped dark cellular debris comprised of a thin and electron-dense outer layer and less dense inner layer containing multiple hole-like structures. In these structures, OPN expression was observed along the periphery and hole-like structures, some of which contained electron-dense mitochondria-like profiles (blue arrowheads in **e** and **f**). M, microglial cells. (**g–i**) Confocal microscope images of a semi-thin section labeled for OPN (**g**), the overlay image of the confocal microscope data (**h**), and the corresponding electron microscope image (**i**). (**j**, **k**) Higher magnification image of the boxed area in **i**, showing that OPN protein, as indicated by silver-enhanced immunogold particles, was specifically localized on the surface (black arrows) of the outer compact layer and hole-like structures within dark cellular debris. Note that in the latter, OPN signals were evident on their peripheral outline (magenta arrows) and mitochondria-like profiles (blue arrowheads) inside. Scale bars = 2 μm for **a–c**; 1 μm for **d**, **j**; 0.25 μm for **e**; 0.5 μm for **f**, **k**; 5 μm for **g–i**
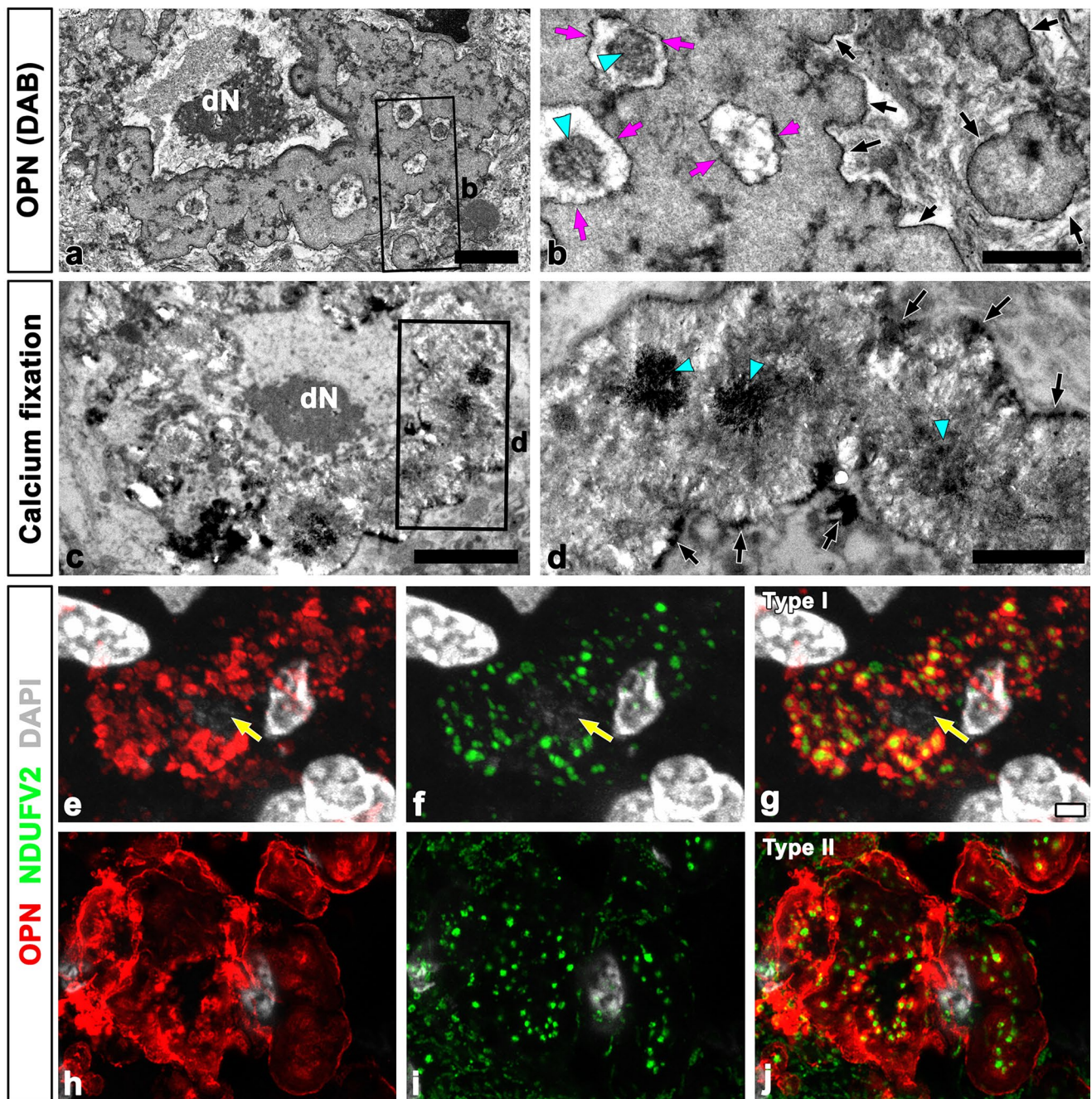
Fig. 6 Ultrastructural identification of type II OPN deposits in the pyramidal cell layer of the CA1 hippocampus by comparison of pre-embedding immunoelectron microscopy and the osmium/potassium dichromate method. (**a**) Pre-embedding electron microscopic images immunostained with OPN, showing an irregularly shaped cell debris consisting of nuclear chromatin-like materials (dN) and outer cytoplasmic parts with high electron density. (**b**) Higher magnification image of the boxed area in **a**, showing that the cytoplasmic part had several electron-transparent holes, in which small and electron-dense mitochondria-like structures (blue arrowheads) were present. Note that electron-dense DAB grains were evident along the periphery of the cell debris (black arrows) and also on the wall (magenta arrows) and mitochondria-like structures (blue arrowheads) of the holes. (**c**) Representative images acquired using the osmium/potassium dichromate method, showing a calcified body that was entirely composed of aggregates of needle- or rod-shaped electron-dense calcium crystals and had centrally located nuclear chromatin-like materials (dN). (**d**) Higher magnification image of the boxed area in **c**, showing that calcium crystals were more densely present along the periphery of the calcified body (black arrows) and within mitochondria-like structures (blue arrowheads). (**e–j**) Double labeling for OPN and the mitochondria marker NADH dehydrogenase flavoprotein 2 (NDUFV2) in the type I (**e–g**) and type II (**h–j**) OPN deposits. OPN-positive dots and NDUFV2 shared an overlapping distribution in the type I OPN deposits surrounding the weakly DAPI-labeled nuclei (yellow arrows in **e–g**). Note that OPN dots scattered in the interior of the type II OPN deposits were co-localized with NDUFV2, while OPN expression observed along their periphery was not associated with NDUFV2. DAPI was used for nuclear counterstain. Scale bars = 2 μm for **a**, **e–j**; 1 μm for **b–d**
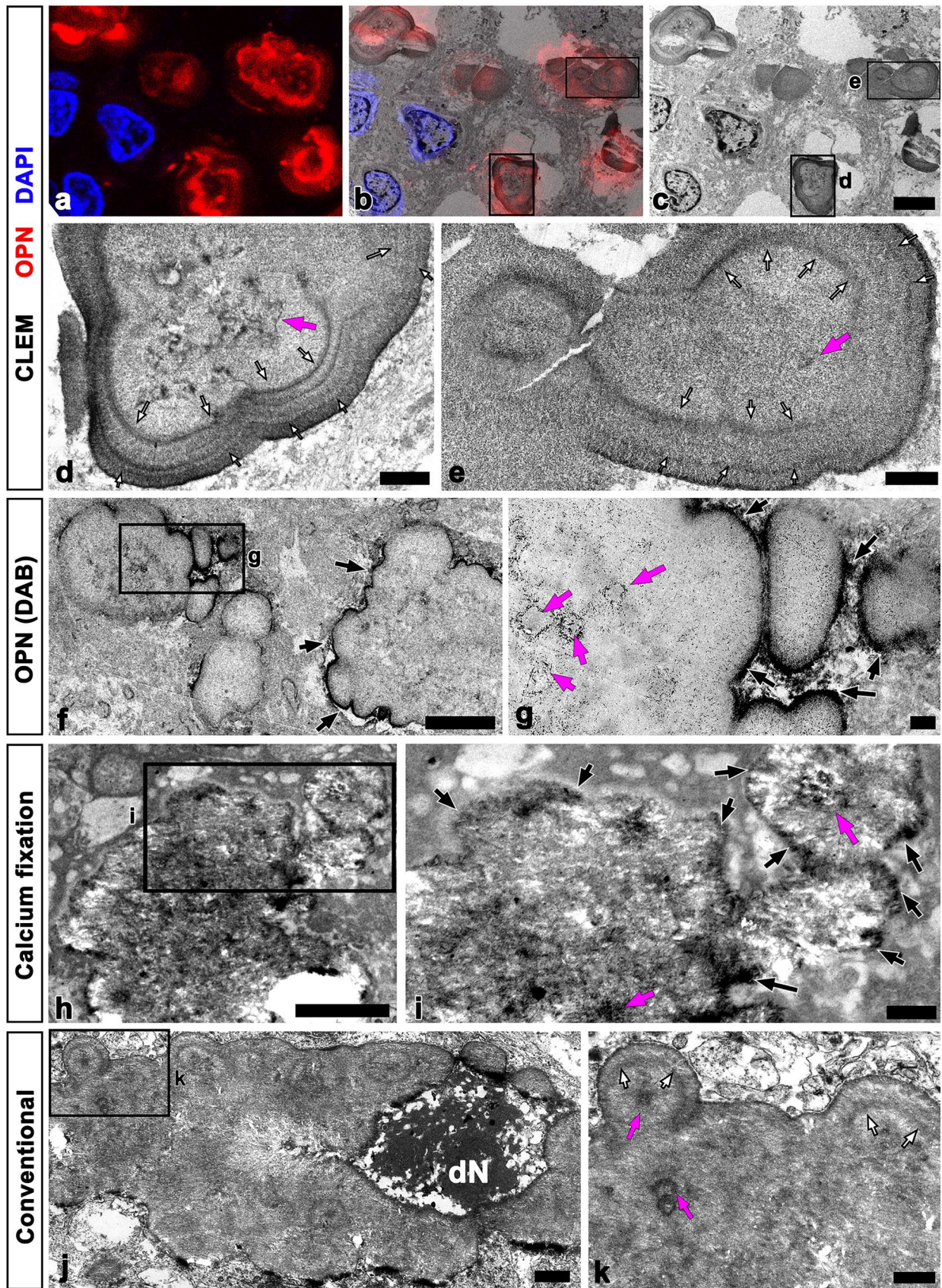
◄Fig. 7 Ultrastructural identification of type III OPN deposits in the pyramidal cell layer of the CA1 hippocampus using various ultrastructural analyses. (**a–c**) Confocal microscope images of a semi-thin section labeled for OPN (**a**), the overlay image of the confocal microscope data (**b**), and the corresponding electron microscope image (**c**). (**d**, **e**) Higher magnification images of the boxed areas in **c**. Notably, the type III OPN deposits consisted of the periphery with concentric lamellae (white arrows in **d** and **e**) of compact fibrils, and the center with less compact fibrils and electron-dense bodies (magenta arrows in **d** and **e**). (**f**, **g**) Lower (**f**) and higher (**g**) magnification images from pre-embedding immunoelectron microscopy, showing that OPN staining was intense at the periphery of large irregular-shaped structures (black arrows in **f** and **g**) and centrally located bodies (magenta arrows in **g**). Note that small acellular bodies appeared to be attached to the periphery of this structure. (**h**, **i**) Representative electron microscopic images acquired using the osmium/potassium dichromate method, showing a large calcifying body consisting of adjacent small calcifying bodies that had fused to each other. The boxed area in **h** was enlarged in **i**. Note that needle-like calcium crystals were present throughout the entire structure of the calcified bodies, and that more intense calcium crystals were localized along their periphery (black arrows) and unidentifiable profiles inside (magenta arrows). (**j**, **k**) Conventional electron microscopic images of the CA1 pyramidal cell layer, showing what appeared to be a calcifying body that had centrally located nuclear chromatin-like materials (dN) and compacted as well as laminated structures (white arrows in **k**) located in the periphery. The boxed area in **j** was enlarged in **k**. Scale bars=5 μm for **a–c**; 1 μm for **d–e**, **j**; 0.5 μm for **f–g**, **i**, **k**; 2 μm for **h**

previously reported that some neurons in the pyramidal cell layer became dark and condensed and retain their compact ultrastructure 4 weeks after reperfusion (Riew et al. 2016). In particular, these dark neurons had some mitochondria that retained their cristae structures until the moment of neuronal disintegration, and these mitochondria were filled with densely packed needle-shaped crystals, which strongly corroborates the present data. Thus, supporting and extending our previous observations, the present study provides evidence of a further calcium precipitation process beyond the mitochondria in the perikarya of these dark neurons.

Previous studies have shown that CA1 non-pyramidal interneurons are relatively resistant to transient ischemic insults (Fukuda et al. 1993; Tortosa and Ferrer 1993); they have been shown to survive up to six weeks after ischemia, while consistently undergoing degenerative changes resembling the type I OPN deposit-laden cells in our study. More specifically, they were shrunken with hyperchromatic nuclei and had electron-dense cytoplasm with obscure boundaries. In addition, PV interneurons, a subpopulation of the GABAergic interneurons, are resistant at early time points after an ischemic insult, but a delayed death is induced up to 14 days after ischemia (Himeda et al. 2005), which suggests that TUNEL-positive degenerating neurons in the present study could be PV interneurons. Although TUNEL-positive cells with cytoplasm filled with type I OPN deposits were devoid of PV expression in the CA1 hippocampus of

reperfused rats at 4 weeks (see Fig. 4e–h), this could be explained by the report that conspicuous reduction of PV expression is noted in interneurons during 5–14 days after ischemia (Himeda et al. 2005). Since PV is a calcium-binding protein, PV interneurons could have been protected from cytotoxic calcium in the acute phase by its calcium buffering capacity. However, excess calcium might have eventually caused the deposition of OPN-labeled ectopic calcification in delayed phases, as observed in type II and III OPN-laden structures. The detailed molecular mechanisms underlying ectopic calcification process remain to be elucidated.

Corpora amylacea represents a spherical structure with an average diameter of 15 μm that accumulates primarily in the periventricular and subpial regions of the human brain during the aging process and in some neurodegenerative diseases (Nishio et al. 2001; Pisa et al. 2016; Ramsey 1965; Riba et al. 2021; Sakai et al. 1969). Notably, we found that the OPN deposits had the following features similar to corpora amylacea, despite their differences in localization and size. Both structures were composed of tightly aggregated fibrils with a concentrically laminated layer, contained morphologically preserved mitochondria, and showed positive PAS reaction and ubiquitin expression (Augé et al. 2019, 2018b; Cissé et al. 1991; Navarro et al. 2018; Pisa et al. 2018; Song et al. 2014). In addition, the core of the corpora amylacea was formed by calcium salts, including calcium phosphate and calcium oxalate (Kodaka et al. 2008; Magura and Spector 1979; Nakamura et al. 1995), and the possibility that corpora amylacea is formed from augmented iron deposition and mitochondrial insufficiency in the brain has also been suggested (Schipper 2004). In particular, Auge et al. showed that immature corpora amylacea are composed of randomly oriented fibers and contain mitochondria as well as cellular debris in the core, whereas in mature corpora amylacea, the fibrillary structures become compacted and increase in number, indicating that the OPN deposits and corpora amylacea share similar ultrastructural features during their maturation (Augé et al. 2019).

Corpora amylacea was first reported in the brains of elderly patients in 1837 (Catola and Achúcarro 1906), but their origin and function have only recently been elucidated. Several studies have shown that corpora amylacea acts as a waste substance container in which deleterious or residual products are isolated and later eliminated from the nervous system (Augé et al. 2017, 2019; Navarro et al. 2018; Riba et al. 2019, 2021). The cellular origin of corpora amylacea has not been clarified yet; however, some studies have reported that corpora amylacea is derived from a glial source in that it is located within astrocytic processes (Augé et al. 2019; Leel-Ossy 2001; Manich et al. 2016; Navarro et al. 2018; Palmucci et al. 1982; Ramsey 1965; Sbarbati et al.
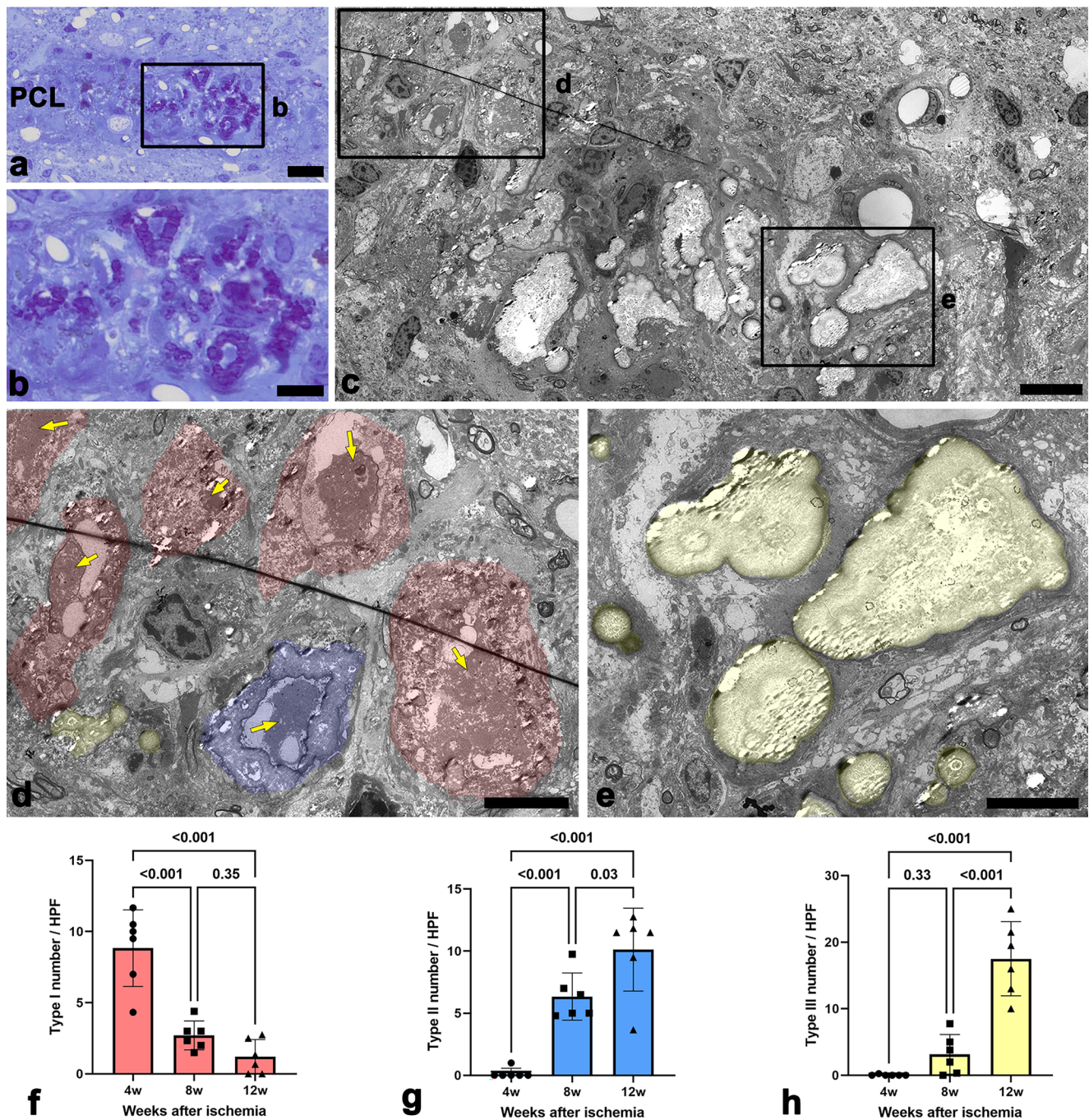
Fig. 8 Quantitative temporal analysis of three types of OPN deposits in the pyramidal cell layer of the ischemic CA1 hippocampus. (**a**, **b**) Light microscopic images from toluidine blue-stained semi-thin section from the CA1 pyramidal cell layer at 8 weeks after ischemia. The boxed area in **a** was enlarged in **b**. Note that several OPN deposits variable in size and shape were scattered in the CA1 pyramidal cell layer. (**c–e**) Conventional electron microscopic images from the adjacent ultrathin sections from the same epon blocks, showing that all types of OPN deposits including type I (shaded in red), type II (shaded in blue), and type III (shaded in yellow) OPN deposits were observed in the CA1 pyramidal cell layer of the same animal. The

boxed areas in **c** were enlarged in **d** and **e**. Yellow arrows in **d** denote the nuclear chromatin-like materials. (**f–h**) Quantitative analysis of the time-dependent number of three types of OPN deposits in the CA1 pyramidal cell layer, showing that the numbers of type I deposits gradually decreased from 4 to 12 weeks after ischemia, while both type II and III deposits were rarely detected at 4 weeks, but increased during the subsequent injury period ($n = 3$–5 sections from 6 to 8 rats per time points, one-way ANOVA with Tukey's multiple comparison test). The data are expressed as mean ± SEM and the numbers on each bar graph indicate the p values. Scale bars = 20 μm for **a**; 10 μm for **b–c**; 5 μm for **d–e**

Table 1 Classification criteria for the three types of OPN deposits in the CA1 hippocampus of ischemic rats

Defining criteria		Type I OPN deposits	Type II OPN deposits	Type III OPN deposits
OPN expression	Light microscopic findings	Granular puncta Localized to the perinuclear region	Larger, variable in size and shape Absence of limited cell boundaries	Smooth-outlined, concentrically laminated structures Clusters of deposits
	Ultrastructural localization	Mitochondria (co-localized with NDUFV2)	Periphery of cellular debris Mitochondria (co-localized with NDUFV2)	Periphery of deposit conglomerate Unidentifiable profiles inside (probably calcifying mitochondria)
Calcium deposition		Confined to mitochondria	Entire structure with prominent calcium at the periphery and mitochondria	Entire structure with intense calcium at the periphery and unidentifiable profiles inside
Ultrastructural identification of OPN deposit-laden structures		Degenerated neuron retaining cell shape with condensed nuclei Mitochondria with recognizable cristae	Irregularly shaped cellular debris with condensed nuclei Electron-dense mitochondria-like profiles	Smooth-outlined structures consisting of a periphery with concentric lamellae of compact fibrils and a center with less compact fibrils and electron dense bodies Unidentifiable mitochondria

OPN osteopontin, *NDUFV2* nicotinamide adenine dinucleotide dehydrogenase (ubiquinone) flavoprotein 2

1996). On the other hand, intra-axonal corpora amylacea surrounded by myelin-like structures have been found in amyotrophic lateral sclerosis (ALS) and the aged human CNS, and the presence of neuronal proteins like neurofilaments, microtubule-associated protein 2, and β tubulin III have been confirmed in the corpora amylacea (Mizutani et al. 1987; Notter and Knuesel 2013, Selmaj et al. 2008; Takahashi et al. 1975; Wilhelmus et al. 2011). Furthermore, Doehner et al. showed that the deposition of corpora amylacea-like structures is due to cellular debris budding off from aged neurons, which are associated with neuritic swelling with degenerating mitochondria (Doehner et al. 2012). Thus, we postulate that type I OPN deposits reorganize into corpora amylacea-like structures as they evolve into type II and III deposits while processing deleterious neuronal debris.

In addition to neuronal proteins, corpora amylacea is known to be immunoreactive with cytoskeletal proteins, mitochondrial proteins, complement cascade components, and microbial proteins (Augé et al. 2018a, 2019; Botez and Rami, 2001; Doehner et al. 2012; Pisa et al. 2016; Wilhelmus et al. 2011). However, we are the first to demonstrate that OPN, a matricellular protein known to be involved in ectopic calcification and neuroinflammation, is a component of the corpora amylacea, by linking its distinct ultrastructure with molecular and histochemical characteristics using CLEM (Park et al. 2012; Riew

et al. 2017, 2019). In addition, the entire process of corpora amylacea formation by ischemia was elucidated through OPN deposition as a surrogate marker; thus, our study could help clarify the origin and development of human corpora amylacea in aging and neurodegeneration.

It is also important to consider that focal and global forebrain ischemias share the basic mechanisms leading to cell death, but there are important differences in their pathophysiology (Barreto et al. 2011; Nedergaard and Dirnagl 2005; Takano et al. 2009). Focal ischemia induces pan-necrosis of all cell types in the infarct core, while global ischemia leads to delayed cell death in the hippocampus with preservation of astrocytes and microglia, which become activated. Considering that astrocytes and microglia participate in the accumulation and structural expansion of calcium deposits (Gayoso et al. 2003; Oliveira et al. 2003), and that heterogeneity of astroglial population is a contributing factor to variations in regional vulnerability to neurodegeneration and calcium deposition (Rodríguez et al. 2004), the formation of OPN deposits and calcification can be promoted in this model of global forebrain ischemia rather than in other acute brain insult models, including focal ischemia. Therefore, the formation of the OPN deposits related to neurodegeneration may not be considered a generalized phenomenon during acute CNS insults.
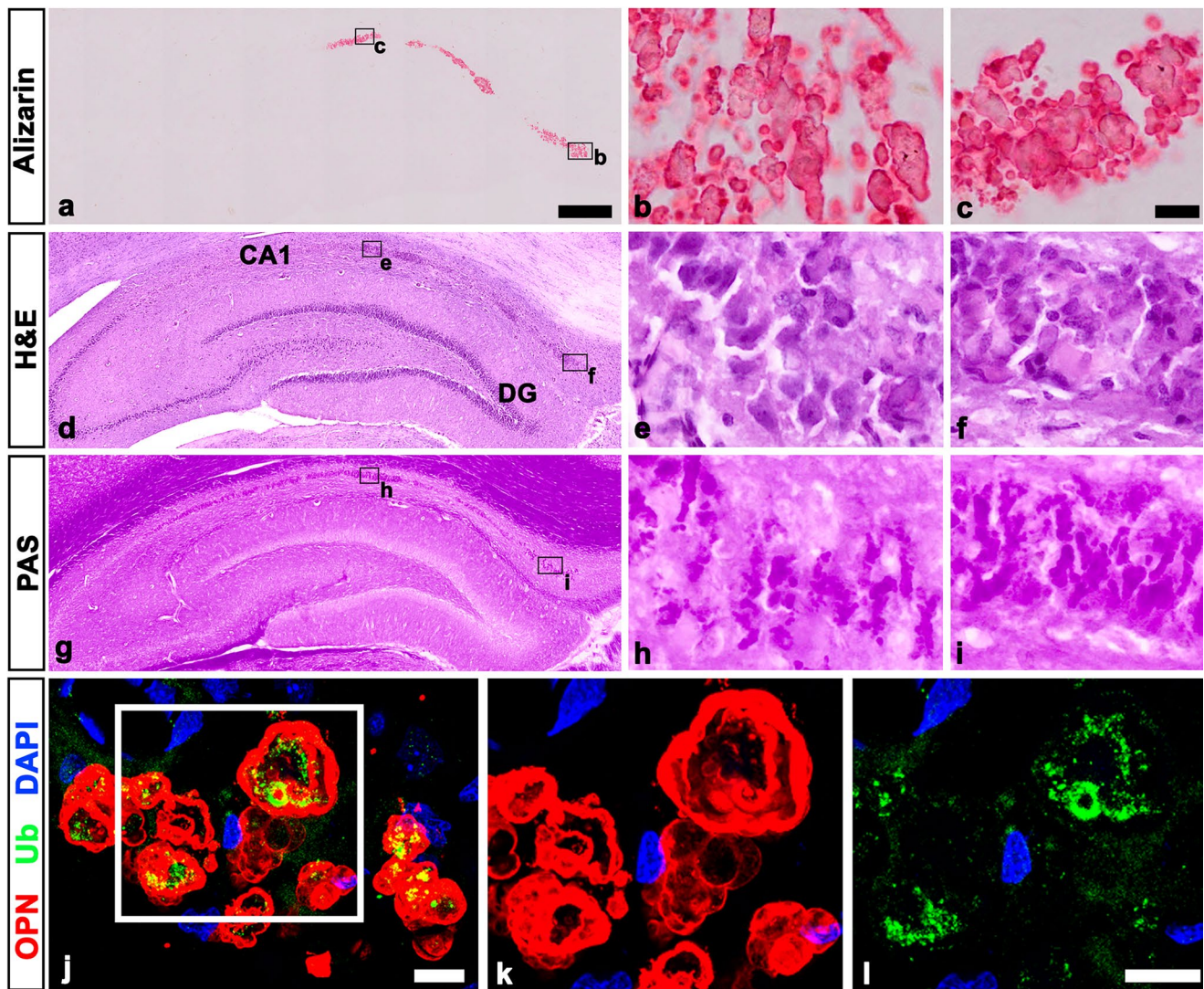
Fig. 9 Relationship between the OPN deposits and the corpora amylacea in the pyramidal cell layer of the ischemic CA1 hippocampus. (**a–i**) Serial sections from ischemic hippocampus at 8 weeks post-ischemia were stained with Alizarin Red (**a–c**), hematoxylin and eosin (H&E; **d–f**), and periodic acid-Schiff (PAS; **g–i**). The boxed areas in **a**, **d**, and **g** were enlarged in **b**, **c**, **e**, **f**, **h**, and **i**, respectively. Note that extracellular aggregates stained with H&E, PAS, and Alizarin Red, respectively, in the CA1 pyramidal cell layer were remarkably similar in distribution pattern, shape, and size. DG, dentate gyrus. (**j–l**). Double labeling of OPN and ubiquitin in the CA1 pyramidal cell layer, showing that ubiquitin was mainly localized to the central part of OPN-positive deposits. DAPI was used for nuclear counterstain. Scale bars = 400 μm for **a**, **d**, **g**; 20 μm for **b–c**, **e–f**, **h–i**; 10 μm for **j–l**

In conclusion, our data demonstrate that ischemic insults induced the formation of three different types of OPN deposits in the pyramidal cell layer of the CA1 hippocampus over a chronic interval of 4–12 weeks. The morphological changes of OPN deposits may represent a series of processes forming the corpora amylacea-like structure, in which selective calcium deposits initially occurred in the mitochondria with subsequent propagation of calcification occurring throughout the structures, suggesting that OPN may play an important role in such processes.
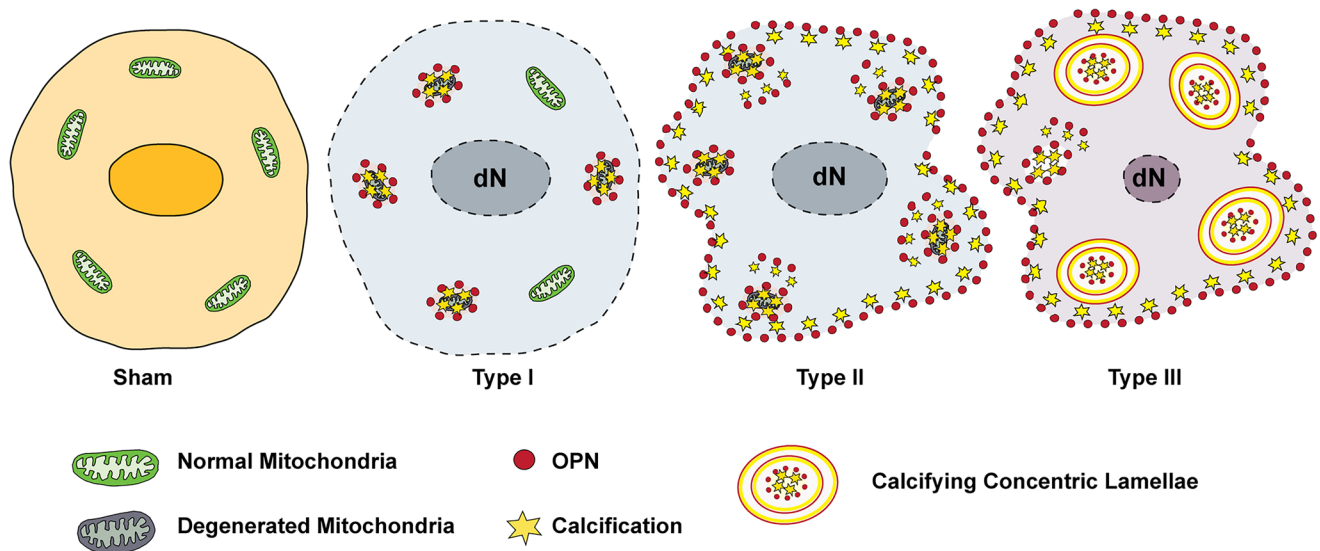
Fig. 10 Schematic diagram of the process by which three types of OPN deposits are formed from degenerating neurons in the CA1 hippocampus after ischemia. Type I OPN deposits were degenerative calcified mitochondria that accumulated within the dark cells with irregularly shaped nuclei (dN) but maintained their cell shape. Type II deposits were calcified dead cells with amorphous structures, where OPN expression was prominent on their peripheral outline and within degenerative mitochondria-like structures. Type III deposits were large calcifying deposits with concentric, laminated structures and OPN expression intense at the periphery and with irregularly shaped bodies in the center of the deposits

Declarations

Ethics approval All experimental protocols and animal care provisions were in accordance with the Laboratory Animals Welfare Act, the Guide for the Care and Use of Laboratory Animals, and the Guidelines and Policies for Rodent Survival Surgery provided by the Institutional Animal Care and Use Committee (IACUC) at the College of Medicine of The Catholic University of Korea (approval number: CUMS-2020–0041-03).

Competing interests The authors declare no competing interests.

References

An J, Yang H, Yang E, Chung S, Kim DY, Jou I, Park SM, Kim BG, Chwae YJ, Joe EH (2021) Dying neurons conduct repair processes in the injured brain through osteopontin expression in cooperation with infiltrated blood monocytes. Glia 69:1037–1052

Augé E, Bechmann I, Llor N, Vilaplana J, Krueger M, Pelegrí C (2019) Corpora amylacea in human hippocampal brain tissue are intracellular bodies that exhibit a homogeneous distribution of neoepitopes. Sci Rep 9:2063

Augé E, Cabezón I, Pelegrí C, Vilaplana J (2017) New perspectives on corpora amylacea in the human brain. Sci Rep 7:41807

Augé E, Duran J, Guinovart JJ, Pelegrí C, Vilaplana J (2018a) Exploring the elusive composition of corpora amylacea of human brain. Sci Rep 8:13525

Augé E, Pelegrí C, Manich G, Cabezón I, Guinovart JJ, Duran J, Vilaplana J (2018b) Astrocytes and neurons produce distinct types of polyglucosan bodies in Lafora disease. Glia 66:2094–2107

Barreto G, White RE, Ouyang Y, Xu L, Giffard RG (2011) Astrocytes: targets for neuroprotection in stroke. Cent Nerv Syst Agents Med Chem 11:164–173

Bendel O, Bueters T, von Euler M, Ove Ogren S, Sandin J, von Euler G (2005) Reappearance of hippocampal CA1 neurons after ischemia is associated with recovery of learning and memory. J Cereb Blood Flow Metab 25:1586–1595

Bonnekoh P, Kuroiwa T, Kloiber O, Hossmann K (1992) Time profile of calcium accumulation in hippocampus, striatum and frontoparietal cortex after transient forebrain ischemia in the gerbil. Acta Neuropathol 84:400–406

Botez G, Rami A (2001) Immunoreactivity for Bcl-2 and C-Jun/AP1 in hippocampal corpora amylacea after ischaemia in humans. Neuropathol Appl Neurobiol 27:474–480

Bueters T, von Euler M, Bendel O, von Euler G (2008) Degeneration of newly formed CA1 neurons following global ischemia in the rat. Exp Neurol 209:114–124

Catola G, Achúcarro N (1906) Über die Entstehung der Amyloidkörperchen im Zentralnervensystem. Virchows Archiv Für Pathologische Anatomie Und Physiologie Und Für Klinische Medizin 184:454–469

Cavanagh JB (1999) Corpora-amylacea and the family of polyglucosan diseases. Brain Res Brain Res Rev 29:265–295

Choi JS, Kim HY, Cha JH, Choi JY, Lee MY (2007) Transient microglial and prolonged astroglial upregulation of osteopontin following transient forebrain ischemia in rats. Brain Res 1151:195–202

Cissé S, Lacoste-Royal G, Laperrière J, Cabana T, Gauvreau D (1991) Ubiquitin is a component of polypeptides purified from corpora amylacea of aged human brain. Neurochem Res 16:429–433

de Coo R, Buddiger P, Smeets H, Geurts van Kessel A, Morgan-Hughes J, Weghuis DO, Overhauser J, van Oost B (1995) Molecular

cloning and characterization of the active human mitochondrial NADH:ubiquinone oxidoreductase 24-kDa gene (NDUFV2) and its pseudogene. Genomics 26:461–466

Doehner J, Genoud C, Imhof C, Krstic D, Knuesel I (2012) Extrusion of misfolded and aggregated proteins–a protective strategy of aging neurons? Eur J Neurosci 35:1938–1950

Ellison JA, Barone FC, Feuerstein GZ (1999) Matrix remodeling after stroke. De novo expression of matrix proteins and integrin receptors. Ann N Y Acad Sci 890:204–222

Ellison JA, Velier JJ, Spera P, Jonak ZL, Wang X, Barone FC, Feuerstein GZ (1998) Osteopontin and its integrin receptor alpha(v)beta3 are upregulated during formation of the glial scar after focal stroke. Stroke 29:1698–1706; discussion 1707

Fukuda T, Nakano S, Yoshiya I, Hashimoto PH (1993) Persistent degenerative state of non-pyramidal neurons in the CA1 region of the gerbil hippocampus following transient forebrain ischemia. Neuroscience 53:23–38

Gayoso MJ, Al-Majdalawi A, Garrosa M, Calvo B, Díaz-Flores L (2003) Selective calcification of rat brain lesions caused by systemic administration of kainic acid. Histol Histopathol 18:855–869

Gliem M, Krammes K, Liaw L, van Rooijen N, Hartung HP, Jander S (2015) Macrophage-derived osteopontin induces reactive astrocyte polarization and promotes re-establishment of the blood brain barrier after ischemic stroke. Glia 63:2198–2207

Himeda T, Hayakawa N, Tounai H, Sakuma M, Kato H, Araki T (2005) Alterations of interneurons of the gerbil hippocampus after transient cerebral ischemia: effect of pitavastatin. Neuropsychopharmacology 30:2014–2025

Jin YC, Lee H, Kim SW, Kim ID, Lee HK, Lee Y, Han PL, Lee JK (2016) Intranasal delivery of RGD motif-containing osteopontin icosamer confers neuroprotection in the postischemic brain via alphavbeta3 integrin binding. Mol Neurobiol 53:5652–5663

Kim HL, Riew TR, Park J, Lee Y, Kim IB (2021) Correlative light and electron microscopy using frozen section obtained using cryo-ultramicrotomy. Int J Mol Sci 22:4273

Kirino T, Sano K (1984) Selective vulnerability in the gerbil hippocampus following transient ischemia. Acta Neuropathol 62:201–208

Kiryk A, Pluta R, Figiel I, Mikosz M, Ulamek M, Niewiadomska G, Jablonski M, Kaczmarek L (2011) Transient brain ischemia due to cardiac arrest causes irreversible long-lasting cognitive injury. Behav Brain Res 219:1–7

Kodaka T, Hirayama A, Sano T, Debari K, Mayahara M, Nakamura M (2008) Fine structure and mineral components of primary calculi in some human prostates. J Electron Microsc (tokyo) 57:133–141

Lee MY, Choi YS, Choi JS, Min DS, Chun MH, Kim ON, Lee SB, Kim SY (2002) An immunohistochemical study of APG-2 protein in the rat hippocampus after transient forebrain ischemia. Brain Res 924:237–241

Lee MY, Shin SL, Choi YS, Kim EJ, Cha JH, Chun MH, Lee SB, Kim SY (1999) Transient upregulation of osteopontin mRNA in hippocampus and striatum following global forebrain ischemia in rats. Neurosci Lett 271:81–84

Leel-Ossy L (2001) New data on the ultrastructure of the corpus amylaceum (polyglucosan body). Pathol Oncol Res 7:145–150

Maetzler W, Berg D, Funke C, Sandmann F, Stunitz H, Maetzler C, Nitsch C (2010) Progressive secondary neurodegeneration and microcalcification co-occur in osteopontin-deficient mice. Am J Pathol 177:829–839

Magura CE, Spector M (1979) Scanning electron microscopy of human prostatic corpora amylacea and corpora calculi, and prostatic calculi. Scan Electron Microsc 713–720

Manich G, Cabezón I, Augé E, Pelegrí C, Vilaplana J (2016) Periodic acid-Schiff granules in the brain of aged mice: From amyloid aggregates to degenerative structures containing neo-epitopes. Ageing Res Rev 27:42–55

Meller R, Stevens SL, Minami M, Cameron JA, King S, Rosenzweig H, Doyle K, Lessov NS, Simon RP, Stenzel-Poore MP (2005) Neuroprotection by osteopontin in stroke. J Cereb Blood Flow Metab 25:217–225

Mizutani T, Satoh J, Morimatsu Y (1987) Axonal polyglucosan body in the ventral posterolateral nucleus of the human thalamus in relation to ageing. Acta Neuropathol 74:9–12

Mori F, Tanji K, Wakabayashi K (2000) Widespread calcium deposits, as detected using the Alizarin Red S technique, in the nervous system of rats treated with dimethyl mercury. Neuropathology 20:210–215

Morikawa S, Sato A, Ezaki T (2018) A simple, one-step polychromatic staining method for epoxy-embedded semithin tissue sections. Microscopy (oxf) 67:331–344

Nakamura S, Akiguchi I, Seriu N, Ohnishi K, Takemura M, Ueno M, Tomimoto H, Kawamata T, Kimura J, Hosokawa M (1995) Monoamine oxidase-B-positive granular structures in the hippocampus of aged senescence-accelerated mouse (SAMP8). Acta Neuropathol 90:626–632

Navarro PP, Genoud C, Castaño-Díez D, Graff-Meyer A, Lewis AJ, de Gier Y, Lauer ME, Britschgi M, Bohrmann B, Frank S, Hench J, Schweighauser G, Rozemuller AJM, van de Berg WDJ, Stahlberg H, Shahmoradian SH (2018) Cerebral corpora amylacea are dense membranous labyrinths containing structurally preserved cell organelles. Sci Rep 8:18046

Nedergaard M, Dirnagl U (2005) Role of glial cells in cerebral ischemia. Glia 50:281–286

Nishio S, Morioka T, Kawamura T, Fukui K, Nonaka H, Matsushima M (2001) Corpora amylacea replace the hippocampal pyramidal cell layer in a patient with temporal lobe epilepsy. Epilepsia 42:960–962

Nitsch C, Scotti AL (1992) Ibotenic acid-induced calcium deposits in rat substantia nigra. Ultrastructure of their time-dependent formation. Acta Neuropathol 85:55–70

Notter T, Knuesel I (2013) Reelin immunoreactivity in neuritic varicosities in the human hippocampal formation of non-demented subjects and Alzheimer's disease patients. Acta Neuropathol Commun 1:27

Oliveira A, Hodges H, Rezaie P (2003) Excitotoxic lesioning of the rat basal forebrain with S-AMPA: consequent mineralization and associated glial response. Exp Neurol 179:127–138

Ordy JM, Wengenack TM, Bialobok P, Coleman PD, Rodier P, Baggs RB, Dunlap WP, Kates B (1993) Selective vulnerability and early progression of hippocampal CA1 pyramidal cell degeneration and GFAP-positive astrocyte reactivity in the rat four-vessel occlusion model of transient global ischemia. Exp Neurol 119:128–139

Palmucci L, Anzil AP, Luh S (1982) Intra-astrocytic glycogen granules and corpora amylacea stain positively for polyglucosans: a cytochemical contribution on the fine structural polymorphism of particulate polysaccharides. Acta Neuropathol 57:99–102

Park JM, Shin YJ, Kim HL, Cho JM, Lee MY (2012) Sustained expression of osteopontin is closely associated with calcium deposits in the rat hippocampus after transient forebrain ischemia. J Histochem Cytochem 60:550–559

Pisa D, Alonso R, Rábano A, Carrasco L (2016) Corpora amylacea of brain tissue from neurodegenerative diseases are stained with specific antifungal antibodies. Front Neurosci 10:86

Pisa D, Alonso R, Marina AI, Rábano A, Carrasco L (2018) Human and microbial proteins from corpora amylacea of Alzheimer's disease. Sci Rep 8:9880

Probst W (1986) Ultrastructural localization of calcium in the CNS of vertebrates. Histochemistry 85:231–239

Pulsinelli WA, Brierley JB (1979) A new model of bilateral hemispheric ischemia in the unanesthetized rat. Stroke 10:267–272

Pulsinelli WA, Brierley JB, Plum F (1982) Temporal profile of neuronal damage in a model of transient forebrain ischemia. Ann Neurol 11:491–498

Radenovic L, Nenadic M, Ułamek-Kozioł M, Januszewski S, Czuczwar SJ, Andjus PR, Pluta R (2020) Heterogeneity in brain distribution of activated microglia and astrocytes in a rat ischemic model of Alzheimer's disease after 2 years of survival. Aging (albany NY) 12:12251–12267

Ramonet D, de Yebra L, Fredriksson K, Bernal F, Ribalta T, Mahy N (2006) Similar calcification process in acute and chronic human brain pathologies. J Neurosci Res 83:147–156

Ramonet D, Pugliese M, Rodriguez MJ, de Yebra L, Andrade C, Adroer R, Ribalta T, Mascort J, Mahy N (2002) Calcium precipitation in acute and chronic brain diseases. J Physiol Paris 96:307–312

Ramsey HJ (1965) Ultrastructure of corpora amylacea. J Neuropathol Exp Neurol 24:25–39

Riba M, Augé E, Campo-Sabariz J, Moral-Anter D, Molina-Porcel L, Ximelis T, Ferrer R, Martín-Venegas R, Pelegrí C, Vilaplana J (2019) Corpora amylacea act as containers that remove waste products from the brain. Proc Natl Acad Sci U S A 116:26038–26048

Riba M, Del Valle J, Augé E, Vilaplana J, Pelegrí C (2021) From corpora amylacea to wasteosomes: History and perspectives. Ageing Res Rev 72:101484

Riew TR, Kim HL, Jin X, Choi JH, Shin YJ, Kim JS, Lee MY (2017) Spatiotemporal expression of osteopontin in the striatum of rats subjected to the mitochondrial toxin 3-nitropropionic acid correlates with microcalcification. Sci Rep 7:45173

Riew TR, Kim S, Jin X, Kim HL, Lee JH, Lee MY (2019) Osteopontin and its spatiotemporal relationship with glial cells in the striatum of rats treated with mitochondrial toxin 3-nitropropionic acid: possible involvement in phagocytosis. J Neuroinflammation 16:99

Riew TR, Shin YJ, Kim HL, Cho JM, Pak HJ, Lee MY (2016) Spatiotemporal progression of microcalcification in the hippocampal CA1 region following transient forebrain ischemia in Rats: An ultrastructural study. PLoS ONE 11:e0159229

Rodríguez MJ, Martínez-Sánchez M, Bernal F, Mahy N (2004) Heterogeneity between hippocampal and septal astroglia as a contributing factor to differential in vivo AMPA excitotoxicity. J Neurosci Res 77:344–353

Sakai M, Austin J, Witmer F, Trueb L (1969) Studies of corpora amylacea. I. Isolation and preliminary characterization by chemical and histochemical techniques. Arch Neurol 21:526–544

Sbarbati A, Carner M, Colletti V, Osculati F (1996) Extrusion of corpora amylacea from the marginal gila at the vestibular root entry zone. J Neuropathol Exp Neurol 55:196–201

Schipper HM (2004) Heme oxygenase expression in human central nervous system disorders. Free Radic Biol Med 37:1995–2011

Schipper HM, Cissé S (1995) Mitochondrial constituents of corpora amylacea and autofluorescent astrocytic inclusions in senescent human brain. Glia 14:55–64

Schroeter M, Zickler P, Denhardt DT, Hartung HP, Jander S (2006) Increased thalamic neurodegeneration following ischaemic cortical stroke in osteopontin-deficient mice. Brain 129:1426–1437

Selmaj K, Pawłowska Z, Walczak A, Koziołkiewicz W, Raine CS, Cierniewski CS (2008) Corpora amylacea from multiple sclerosis brain tissue consists of aggregated neuronal cells. Acta Biochim Pol 55:43–49

Shin YJ, Kim HL, Choi JS, Choi JY, Cha JH, Lee MY (2011) Osteopontin: correlation with phagocytosis by brain macrophages in a rat model of stroke. Glia 59:413–423

Shin YJ, Kim HL, Park JM, Cho JM, Kim CY, Choi KJ, Kweon HS, Cha JH, Lee MY (2012) Overlapping distribution of osteopontin and calcium in the ischemic core of rat brain after transient focal ischemia. J Neurotrauma 29:1530–1538

Smith ML, Bendek G, Dahlgren N, Rosén I, Wieloch T, Siesjö BK (1984) Models for studying long-term recovery following forebrain ischemia in the rat. 2. A 2-vessel occlusion model. Acta Neurol Scand 69:385–401

Song W, Zukor H, Liberman A, Kaduri S, Arvanitakis Z, Bennett DA, Schipper HM (2014) Astroglial heme oxygenase-1 and the origin of corpora amylacea in aging and degenerating neural tissues. Exp Neurol 254:78–89

Takahashi K, Agari M, Nakamura H (1975) Intra-axonal Corpora amylacea in ventral and lateral horns of the spinal cord. Acta Neuropathol 31:151–158

Takano T, Oberheim N, Cotrina ML, Nedergaard M (2009) Astrocytes and ischemic injury. Stroke 40:S8-12

Tortosa A, Ferrer I (1993) Parvalbumin immunoreactivity in the hippocampus of the gerbil after transient forebrain ischaemia: a qualitative and quantitative sequential study. Neuroscience 55:33–43

Trump BF, Smuckler EA, Benditt EP (1961) A method for staining epoxy sections for light microscopy. J Ultrastruct Res 5:343–348

Unal-Cevik I, Kilinc M, Gursoy-Ozdemir Y, Gurer G, Dalkara T (2004) Loss of NeuN immunoreactivity after cerebral ischemia does not indicate neuronal cell loss: a cautionary note. Brain Res 1015:169–174

Wang X, Louden C, Yue TL, Ellison JA, Barone FC, Solleveld HA, Feuerstein GZ (1998) Delayed expression of osteopontin after focal stroke in the rat. J Neurosci 18:2075–2083

Wilhelmus MM, Verhaar R, Bol JG, van Dam AM, Hoozemans JJ, Rozemuller AJ, Drukarch B (2011) Novel role of transglutaminase 1 in corpora amylacea formation? Neurobiol Aging 32:845–856

Yan YP, Lang BT, Vemuganti R, Dempsey RJ (2009) Osteopontin is a mediator of the lateral migration of neuroblasts from the subventricular zone after focal cerebral ischemia. Neurochem Int 55:826–832